US Army Corps
of Engineers
Construction Engineering
Research Laboratory

USACERL Technical Report E-90/15
September 1990
Underground Heat Transfer Algorithms

Algorithms for Slab-on-Grade Heat Transfer Calculations

by
William P. Bahnfleth
JoAnn Amber

A major portion of a building's energy consumption can result from earth-coupled heat transfer processes. Accurate prediction of heat transfer rates through floors, basements, bermed walls, and earth-covered roofs is a critical first step toward effective control of earth-coupled losses. Algorithms currently in use, both manual and numerical procedures, have fundamental flaws that make them unsatisfactory beyond the level of crude estimates. This report describes the development of two new algorithms for slab-on-grade heat loss calculations. A method suitable for manual use employs a geometric scaling based on the ratio of floor area to perimeter length. A multiple input transfer function method appropriate for implementation in energy analysis programs is built on a seven-node model of the floor/ground system. The models were validated through comparison with the results of an hourly, three-dimensional finite difference program.

The results of this study will provide the basis for improving existing estimation methods and building simulation programs for military construction. Improved design and modeling techniques will benefit the Army by (1) increasing the accuracy of sizing calculations for heating, ventilation, and air-conditioning equipment, (2) permitting more confident prediction of foundation and underground structure thermal performance during the design phase, and (3) providing a method to demonstrate life-cycle savings due to energy-conservative design features involving foundation insulation or earth shelter.

REPORT DOCUMENTATION PAGE

Form Approved
OMB No. 0704-0188

1. AGENCY USE ONLY (Leave Blank)	2. REPORT DATE	3. REPORT TYPE AND DATES COVERED
	September 1990	Final

4. TITLE AND SUBTITLE

Algorithms for Slab-On-Grade Heat Transfer Calculations

5. FUNDING NUMBERS

PE 4A161102
PR AT23
WU EB-ER9

6. AUTHOR(S)

William P. Bahnfleth and JoAnn Amber

7. PERFORMING ORGANIZATION NAME(S) AND ADDRESS(ES)

USACERL
PO Box 9005
Champaign, IL 61826-9005

8. PERFORMING ORGANIZATION REPORT NUMBER

USACERL TR E-90/15

9 SPONSORING/MONITORING AGENCY NAME(S) AND ADDRESS(ES)

10. SPONSORING/MONITORING AGENCY REPORT NUMBER

11. SUPPLEMENTARY NOTES

Copies are available from the National Technical Information Service, 5285 Port Royal Road, Springfield, VA 22161.

12a. DISTRIBUTION/AVAILABILITY STATEMENT

Approved for public release; distribution is unlimited.

12b. DISTRIBUTION CODE

13. ABSTRACT (Maximum 200 words)

A major portion of a building's energy consumption can result from earth-coupled heat transfer processes. Accurate prediction of heat transfer rates through floors, basements, bermed walls, and earth-covered roofs is a critical first step toward effective control of earth-coupled losses. Algorithms currently in use, both manual and numerical procedures, have fundamental flaws that make them unsatisfactory beyond the level of crude estimates. This report describes the development of two new algorithms for slab-on-grade heat loss calculations. A method suitable for manual use employs a geometric scaling based on the ratio of floor area to perimeter length. A multiple input transfer function method appropriate for implementation in energy analysis programs is built on a seven-node model of the floor/ground system. The models were validated through comparison with the results of an hourly, three-dimensional finite difference program.

The results of this study will provide the basis for improving existing estimation methods and building simulation programs for military construction. Improved design and modeling techniques will benefit the Army by (1) increasing the accuracy of sizing calculations for heating, ventilation, and air conditioning equipment, (2) permitting more confident prediction of foundation and underground structure thermal performance during the design phase, and (3) providing a method to demonstrate life-cycle savings due to energy-conservative design features involving foundation insulation or earth shelter.

14. SUBJECT TERMS	15. NUMBER OF PAGES
algorithms heat transfer	86
	16. PRICE CODE

17 SECURITY CLASSIFICATION OF REPORT	18 SECURITY CLASSIFICATION OF THIS PAGE	19. SECURITY CLASSIFICATION OF ABSTRACT	20. LIMITATION OF ABSTRACT
Unclassified	Unclassified	Unclassified	SAR

FOREWORD

This study was conducted under Project 4A161102AT23, "Basic Research in Military Construction"; Work Unit EB-ER9, "Underground Heat Transfer Algorithms." The research was performed by the Energy Systems Division (ES), U.S. Army Construction Engineering Research Laboratory (USACERL). Dr. Gilbert Williamson is Chief, USACERL-ES.

COL Everett R. Thomas is Commander and Director of USACERL, and Dr. L.R. Shaffer is Technical Director.

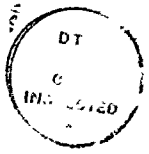

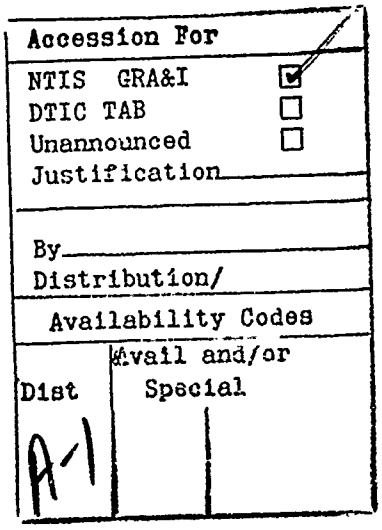

CONTENTS

		Page
	SF298	1
	FOREWORD	2
	LIST OF FIGURES AND TABLES	5
1	INTRODUCTION	9
	Background	10
	Objective	10
	Approach	10
	Mode of Technology Transfer	10
2	DATA BASE DEVELOPMENT	11
	Mathematical Model	11
	Heat Transfer in Soil	11
	Boundary Conditions	11
	Numerical Solution	18
	Simulation Parameters	18
	Climate	18
	Soil Properties	19
	Ground Surface Properties	19
	Building Parameters	20
	Parametric Groups	21
3	CHARACTERISTIC LENGTH METHOD	22
	Overview	22
	Model Description	24
	Shape and Size Effects on Mean Heat Flux	24
	Extension of Model to Transient Heat Flux	26
	Climate Effects	29
	Soil Thermal Property Effects	33
	Effect of Insulation	39
	Summary	42
4	TRANSFER FUNCTION ALGORITHM	43
	Overview	43
	Concept	43
	Model Development	45
	Basic Equations	46
	Geometry	49
	Soil Properties	51
	Inputs	52
	Network Parameter Specification	53
	Description of Test System	53
	Definition of Network Parameters	54
	Final Definition and Testing	54
	Final Definition	54

CONTENTS (Cont'd)

Validation 57
Network Parameters Based on Characteristic Length 63

5 CONCLUSIONS AND RECOMMENDATIONS 73
Slab Heat Loss Characteristics 73
Temporal and Spatial Characteristics 73
Geometric Effects 73
Climate Effects 74
Ground Surface Boundary Condition Effects 74
Soil Property Effects 74
Insulation Effects 74
Modeling Guidelines 75
Evaluation of Candidate Models 75
Characteristic Length Method 75
Transfer Function Model 75
Recommendations 76

REFERENCES 77

APPENDIX: Data Set Used To Evaluate Proposed Models 79

DISTRIBUTION

FIGURES

Number		Page
1	Ground Surface Energy Balance Components	14
2	Daily-Averaged Heat Loss Per Unit Perimeter Length for Large and Small Slabs, Medford, OR	23
3	Heat Loss vs. Perimeter Length for Uninsulated Floors in Medford, OR (15-m-Deep Domain)	23
4	Heat Loss Per Unit Area vs. A/P for Uninsulated Slabs, Medford, OR (15-m-Deep Domain)	25
5	Daily-Averaged Heat Loss Model for a 12 by 12 m Floor in Medford, OR	28
6	Daily Averaged Air and Ground Surface Temperatures for Phoenix, AZ (Potential Evapotranspiration)	31
7	Typical Effects of k and α Variation on Smoothed, Daily-Averaged Heat Loss From a 12 by 12 m Floor	36
8	Influence of Soil Properties on Area Dependence of Floor Heat Loss	37
9	Effects of Thermal Conductivity and Thermal Diffusivity on Phase Lag of Floor Heat Loss	38
10	January Daily Low and Average Floor Surface Temperatures for a 12 by 12 m Uninsulated Floor in Minneapolis, MN	40
11	January Daily Low and Average Floor Surface Temperatures for a 12 by 12 m Floor With 1 m of 2-in.-Thick Perimeter Insulation in Minneapolis, MN	41
12	Smoothed, Daily-Averaged Heat Loss From a 12 by 12 m Minneapolis Slab Floor With Various Insulation Treatments	41
13	Seven-Node Network Model	45
14	Undisturbed Ground Temperature Profile	50
15	Finite Difference Model of Two Square Slabs	54
16	Heat Flux--Minneapolis, MN	58
17	Heat Flux--Medford, OR	59
18	Heat Flux--Philadelphia, PA	59

FIGURES (Cont'd)

Number		Page
19	Heat Flux--Phoenix, AZ	60
20	Heat Flux--6 by 24 Rectangle	61
21	Heat Flux--18 by 112 Rectangle	61
22	Heat Flux--$T_f = T_{oa}$, Minneapolis, MN	64
23	Heat Flux--$T_f = T_{oa}$, Medford, OR	64
24	Heat Flux--$T_f = T_{oa}$, Philadelphia, PA	65
25	Heat Flux--$T_f = T_{oa}$, Phoenix, AZ	65
26	Heat Flux--$T_f = T_{oa}$, 45 by 45, Minneapolis, MN	66
27	Heat Flux--$T_b = T_{ia}$, Minneapolis, MN	67
28	Heat Flux--$T_b = T_{ia}$, Medford, OR	67
29	Heat Flux--$T_b = T_{ia}$, Philadelphia, PA	68
30	Heat Flux--$T_b = T_{ia}$, Phoenix, AZ	68
31	Heat Flux--$T_b = T_{ia}$, 45 by 45, Minneapolis, MN	69
32	Heat Flux--12 by 12	70
33	Heat Flux--6 by 24	70
34	Heat Flux--45 by 45	71
35	Heat Flux--18 by 112	71

TABLES

Number		Page
1	Test Site Geographic and Climatic Data	19
2	Soil Property Sets	20
3	Daily Average Heat Loss Model Coefficients for Medford, OR (15-m-Deep Domain)	29
4	Effect of Lower Boundary Depth on Mean Heat Loss for Uninsulated Floors in Medford, OR	30
5	Mean, Amplitude, and Phase Shift for Models of Daily Averaged Air and Ground Surface Temperatures	30
6	Daily Heat Loss Model Coefficients for Climate Variation Tests (Case by Case)	32
7	Daily Averaged Heat Loss Model Coefficients for Climate Variation Tests (Composite)	33
8	Heat Loss Data for Varied Thermal Property Cases	34
9	Thermal Conductivity Influence on Floor Center and Edge Heat Loss Values for Two Uninsulated Slabs in Philadelphia, PA, January 21	38
10	Comparison of Daily Averaged Heat Loss Model Coefficients for Three Insulation Treatments in Minneapolis, MN	40
11	Results of the GTF Model for Slabs of Different Sizes	58
12	Results of the GTF Model for Various Locations	60
13	Results of the GTF Model for Nonsquare Slabs	62
14	Results of Substituting Daily Average Outdoor Temperature for Daily Average Ground Surface Temperature	63
15	Results of Substituting Constant Indoor Air Temperature for Daily Average Slab Surface Temperature	66
16	Results of GTF Model Using Parameter Sets Based on Empirical Equations	72

ALGORITHMS FOR SLAB-ON-GRADE HEAT TRANSFER CALCULATIONS

1 INTRODUCTION

Background

The impact of earth-coupled heat transfer processes on the energy consumption and thermal comfort of buildings has been a concern to building scientists for more than 40 years. Early studies[1] showed that the basement of a typical U.S. residence accounted for as little as 10 percent of its total energy consumption. Because leaky, lightly insulated above-grade construction was the rule, foundation heat losses could be ignored or estimated roughly with little penalty. The energy crisis during the 1970s led to changes in construction standards that have considerably improved the performance of typical new buildings. Most of these changes in practice affect the above-ground portion of a building, while foundation designs have changed little. As a result, the same foundation that contributed only 10 percent of the heating load on a 1950's building might be responsible for half the load on a comparable contemporary structure.[2] Thus, the need for accurate foundation heat loss models in much greater than in the past,

One practice that has received attention as a method of decreasing building energy consumption is to insulate foundations against earth-coupled heat transfer losses. U.S. Department of Energy (DOE) research suggests that approximately $5 billion in energy could be saved per year by cost-effective insulation of building foundations.[3] Interest also has grown in earth-sheltered construction.[4] Bermed walls and earth-covered roofs can be used both to moderate the outside climate and as thermal storage media; another reason this design is appealing for military construction is that the earth berm may offer additional security.

Successful application of earth shelter technology requires a clear, quantitative understanding of the performance of the earth-sheltered envelope components. However, a satisfactory modeling method for designing such facilities is not available. The theoretical background needed to support accurate models is incomplete. Experimental studies, limited in number and narrow in scope, provide only clues to the general heat transfer behavior of foundations. Analytical methods (those which are distinguishable from numerical methods) deal with simple geometries and boundary conditions. Detailed simulation of foundations still requires computer resources and expertise in numerical methods not commonly available to the building designer. Indeed, computer hardware limitations have restricted most research via numerical modeling to two-dimensional analysis. The differences between two- and three-dimensional analysis are not well understood; however, the limited evidence available indicates that two-dimensional analysis may underestimate heat transfer rates by 30 percent or more.[5] Other aspects

---

[1]H.D. Bareither, A.N. Fleming, and B. E. Alberty, *Temperature and Heat Loss Characteristics of Concrete Floors Laid on the Ground*, Technical Report PB 93920 (University of Illinois Small Homes Council, 1948); R. S. Dill, W. C. Robinson, and H. D. Robinson, *Measurements of Heat Losses From Slab Floors*, Building Materials and Structures Report BMS103 (National Bureau of Standards, 1943).
[2]K. J. Labs et al., *Building Foundation Design Handbook*, DE88-013350 (Department of Energy [DOE], May 1988).
[3]K.J. Labs et al.
[4]F. Moreland, F. Higgs, and J. Shih (Eds.), *Earth Covered Buildings: Technical Notes*, US-DoE CONF-7806138-P1 (DOE, 1979).
[5]K.J. Labs et al.

of modeling, such as the effect of ground surface boundary conditions, soil properties, and deep ground conditions, also have not been investigated thoroughly. Predictions of design models based on this incomplete science vary considerably. For example, MacDonald et al. reported disagreements as large as 1000 percent between the basement heat loss predictions from seven simplified methods.[6] Earth-sheltered technology is likely to remain immature until new models are developed that account for more of the parameters that influence earth-coupled heat transfer.

The U.S. Army designs, builds, and operates a large inventory of buildings that includes some partially and completely below-ground structures. Improved design and simulation techniques for earth-coupled heat transfer will benefit the Army by (1) making equipment sizing calculations more accurate for heating, ventilation, and air-conditioning (HVAC) systems, (2) permitting more confident prediction of foundation and underground structure thermal performance during the design phase, and (3) providing a method to demonstrate life cycle cost savings due to energy-conservative design approaches involving foundation insulation or earth shelter.

Objective

The objective of this work was to develop algorithms with the potential to provide accurate estimates of earth-coupled heat transfer rates from conventional foundations and earth-sheltered or underground buildings.

Approach

The conventional slab-on-grade foundation was studied as a first step toward developing a general modeling capability. A detailed 8760-hr finite difference model of a slab floor was used to generate a large data base of heat transfer results for rectangular and L-shaped floors against which candidate design models could be tested. Parameters varied in these simulations included location, soil properties, aspect ratio, and ground surface conditions. Models were validated with respect to detailed numerical results because of the limited experimental data available for earth-coupled heat transfer. Two types of models were considered: techniques suitable for rapid manual calculation and those appropriate for use in detailed energy analysis models.

Mode of Technology Transfer

It is anticipated that the modeling techniques developed in this 6.1 basic research will be applied directly to building simulation models used within the Army such as the Building Loads Analysis and System Thermodynamics (BLAST) program.[7]

---

[6]G.R. MacDonald, D.E. Claridge, and P.A. Oatman, "A Comparison of Seven Basement Heat Loss Calculation Methods Suitable for Variable-Base Degree-Day Calculations," *ASHRAE Transactions*, Vol 91 (1985), part 1b.

[7]*BLAST 3.0 User's Manual* (Blast Support Office, Department of Mechanical and Industrial Engineering, University of Illinois, April 1986).

2 DATA BASE DEVELOPMENT

This chapter summarizes the characteristics and performance of the three-dimensional, hourly, finite difference model used to build the data base of simulations on which the simplified models discussed in Chapters 3 and 4 are based. The actual model is discussed in more detail elsewhere.[8] Previous studies by Shipp,[9] Speltz,[10] and Speltz and Meixel[11] adopted related modelling approaches. The primary advancement made through the present work is the more complete investigation of three-dimensional effects.

Mathematical Model

Heat Transfer in Soil

The basis for the detailed model was the three-dimensional, transient heat conduction equation without heat generation, i. e.:

$$\rho c \frac{\partial T}{\partial t} = \nabla \cdot (k \cdot \nabla T) \qquad \text{[Eq 1]}$$

Eckert and Pfender[12] have noted that conditions which typically exist in the soil near a building foundation are such that coupled heat and mass transfer can be neglected. Therefore, no explicit account was taken of transport by liquid or vapor in the soil matrix, and soil was assumed to be a homogeneous medium (constant thermal properties). Effects of moisture and phase change may enter such a model through thermal properties and boundary conditions, however. This simplified treatment of the soil makes modeling considerably easier, but the specification of soil properties for a given site remains problematic. In practice, the knowledge of soil composition and moisture distribution needed to establish properties and boundary conditions accurately is seldom available. This problem cannot be solved by modeling.

Boundary Conditions

In most cases, boundary types encountered in the analysis of earth-coupled buildings fall into four categories:

- Earth-coupled building surfaces
- Far-field boundaries

---

[8] W. P. Bahnfleth, *Three-Dimensional Modeling of Heat Transfer From Slab Floors*, Ph.D. Thesis (University of Illinois, May 1989); also published as USACERL Technical Manuscript E-89/11/ADA210826 (July 1989).

[9] P. H. Shipp, *The Thermal Characteristics of Large Earth-Sheltered Structures*, Ph.D. Thesis (University of Minnesota, 1979).

[10] J. J. Speltz, *A Numerical Simulation of Transient Heat Flow in Earth Sheltered Buildings for Seven Selected U.S. Cities*, M.S. Thesis (Trinity University, 1980).

[11] J. J. Speltz and G. D. Meixel, "A Computer Simulation of the Thermal Performance of Earth Covered Roofs," *Proc. Underground Space Conference and Exposition*, Kansas City, MO (Published, 1981).

[12] E. R. G. Eckert and E. Pfender, "Heat and Mass Transfer in Porous Media With Phase Change," *Proc. 6th International Heat Transfer Conference* (Published by?, 1978).

- Deep ground
- Ground surface.

The following discussion describes the heat transfer processes at these boundaries and the mathematical models of them used as boundary conditions on Eq 1 of this study.

Interior Building Surface Conditions. Heat transfer to interior building envelope surfaces occurs through combined convection and radiation. This flux can be approximated by an expression of the form:

$$Q = h_i \cdot A \cdot \left(T_{room} - T_{floor} \right) \qquad \text{[Eq 2]}$$

where T_{room} and T_{floor} are, respectively, room air and floor surface temperatures and h_i is a combined convective-radiative surface conductance [W/m^2-C]. The American Society for Heating, Refrigeration, and Air-Conditioning Engineers (ASHRAE) has published tables of h_i for a variety of surface orientations and emittances.[13] Values appropriate for nonreflective horizontal surface in still air (6.13 and 9.26 W/m^2-C for upward and downward heat flow, respectively) were used throughout this study. Room air temperature was set to 22 °C in all cases.

Far-Field Soil Conditions. Soil conditions that are several building widths removed from the edge of an isolated structure approach those of the undisturbed ground, in which the temperature distribution is a function of depth and time only. This condition is commonly stated as one of zero lateral flux. When applied at a finite distance from the building (as in numerical models), it implies the existence of a mirror image building reflected about the zero flux boundary. When neighboring structures of different shape are too close for an isolated building assumption to apply, they must be modeled explicitly. (Shipp encountered this situation in modeling Williamson Hall on the University of Minnesota campus.)[14] In the present study, an isolated building was assumed.

Deep Ground Conditions. In the deep ground, either zero flux or specified temperature conditions may be applied, depending on circumstances, i. e.:

$$\frac{\partial T}{\partial z} = 0 \quad \text{for} \quad z \rightarrow \infty$$

or:

$$T = \text{constant} \quad \text{at some } z > 0$$

---

[13] *1989 ASHRAE Fundamentals--SI Version* (American Society of Heating, Refrigeration and Air-Conditioning Engineers [ASHRAE], 1989).
[14] P. H. Shipp.

where z is the vertical coordinate, assumed positive into the ground. A specified temperature condition is particularly appropriate when conditions exist that tend to maintain a fixed temperature at a finite depth, such as a high water table. Data summarized by Kusuda and Achenbach[15] show that annual average earth temperature is well approximated by either average air temperature or well-water temperature, irrespective of depth. These data also show that surface conditions are the driving force behind the temperature distribution in the upper few meters of the soil. Consequently, an asymptotic zero flux lower boundary condition is justified in some cases. This choice is most appropriate in the absence of ground temperature data and when the local water table is not likely to be near the surface. The base case boundary condition in the present study was fixed temperature equal to the average air temperature at a depth of 15 m.

Heat Transfer at the Earth's Surface. Heat transfer at the surface of the earth involves coupled processes of conduction from the ground, convection, evaporation, and radiant exchange in both long (sky and ground infrared) and short (solar) wavelength bands. The balance between these modes depends on many parameters, including soil properties, soil moisture content, ground cover, and weather variables. Past studies have shown, both analytically[16] and experimentally,[17] that the result of this complex process can cause ground surface temperatures to differ substantially from the coincident air temperature.

Despite the extensive evidence that surface conditions can and do have a major effect on the temperature level in the ground (and therefore on heat transfer through earth-coupled building components), models of the ground surface in building simulation studies are often oversimplified. More complete models (e.g., Shipp[18]) include solar gain in the surface boundary condition and account for evaporative effects in an *ad hoc* manner. Only the model of Speltz and Meixel,[19] however, deals directly with all of the identified influences on surface energy balance.

The weather data representation used in modeling is closely linked to the model of surface heat transfer employed. Simple boundary condition models, such as those limited to constant film coefficient convection, require only the dry-bulb temperature. In models employing long time steps (say, a week or longer), air temperature often is approximated by a sinusoidal function. In contrast, a detailed model requires frequent input of many weather variables, including dry- and wet-bulb temperatures, barometric pressure, solar radiation, and wind speed. Prior studies indicate that the use of smoothed approximations to outdoor dry-bulb temperature does not cause significant loss of accuracy relative to actual data used in the same model because the thermal mass of the soil damps short-term variations rapidly, even at shallow depths.[20] The important issue of whether a given climate variable should be included or omitted from a model has not been investigated in much detail, however. In part because detailed representations of the surface boundary have not received extensive use, a boundary condition model similar to that of Speltz was employed in the detailed model. Actual hourly weather data were taken from "typical meteorological year" (TMY) tapes.

---

[15]T. Kasuda and P. R. Achenbach, "Earth Temperature and Thermal Diffusivity at Selected Stations in the United States," *ASHRAE Transactions*, Vol 71 (1965), part 1.

[16]R. R. Gilpin and B. K. Wong, " 'Heat-Valve' Effects in the Ground Thermal Regime," *American Society of Mechanical Engineers (ASME) Journal, Heat Transfer*, Vol 98 (1976).

[17]L. W. Gold, "Influence of Surface Conditions on Ground Temperature," *Canadian Journal of Earth Sciences*, Vol 4 (1967); T. Kasuda, "The Effect of Ground Cover on Earth Temperature," *Alternatives in Energy Conservation: The Use of Earth Covered Buildings*, NSF-RA-76006 (National Science Foundation, 1975).

[18]P. H. Shipp.

[19]J. J. Speltz and G. D. Meixel.

[20]L. S. Shen, J. Poliakova, and Y. J. Huang, "Calculation of Building Foundation Heat Loss Using Superposition and Numerical Scaling," *ASHRAE Transactions*, Vol 94 (1988), part 2.

The ground surface boundary condition can be stated mathematically as a specified flux condition on Eq 1:

$$-k\frac{\partial T}{\partial z}\bigg|_{z=0} = G(t) \qquad \text{[Eq 3]}$$

where the flux G(t) is determined by an energy balance at the ground surface. The surface energy balance[21] has the general form:

$$G = R_t - q_{cs} - q_{et} \qquad \text{[Eq 4]}$$

The rate of conduction of heat into the ground (G) is equal to the net radiation absorbed at the ground surface (R_t) less sensible convection (q_{cs}) and evapotranspiration* (q_{et}). Figure 1 shows these fluxes in relation to a control volume at the surface of the earth. Fluxes are positive in the direction of their respective arrows. Procedures for estimating the components of Eq 4 in the present model were drawn from several sources.

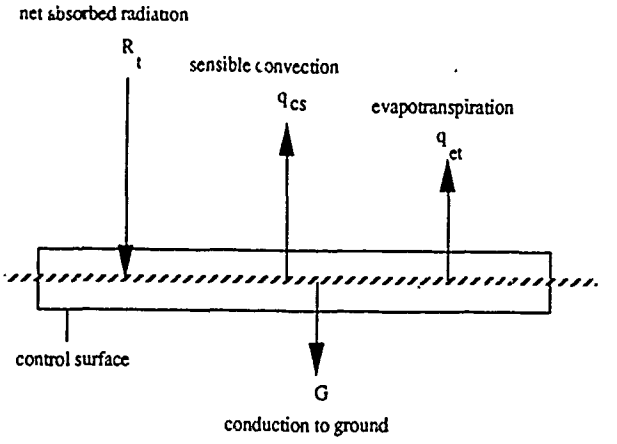

Figure 1. Ground surface energy balance components.

R_t is the sum of absorbed solar radiation (R_{sol}) and incoming infrared sky radiation (R_{sky}) less the infrared radiation emitted by the ground surface (R_g), i.e.:

$$R_t = R_{sol} + R_{sky} - R_g \qquad \text{[Eq 5]}$$

---

[21] W. D. Sellers, *Physical Climatology* (University of Chicago Press, 1965); F. Kreith and W. D. Sellers, "General Principles of Natural Evaporation", *Heat and Mass Transfer in the Biosphere, Part I: Transfer Processes in the Plant Environment*, D. A. DeVries and N. H. Afgan (Eds.).

*Evapotranspiration is an umbrella term denoting all forms of latent heat transport from the ground surface. It includes both evaporation of moisture directly from the soil and transpiration by vegetative ground cover. It also is referred to as "consumptive loss" in some parts of the agriculture literature.

R_{sol} depends on the absorptivity of the ground surface and on incident short-wave radiation, both of which may vary seasonally. The albedo of the ground, α_{sol}, is more commonly tabulated than its complement, the absorptivity, so R_{sol} is determined by application of Eq 6:

$$R_{sol} = (1 - \alpha_{sol}) \cdot R_{sol,i} \qquad \text{[Eq 6]}$$

where $R_{sol,i}$ denotes total solar radiation incident on a horizontal surface, a readily available item of weather data. According to measurements summarized by Sellers,[22] values of α_{sol} vary from as low as 0.05 for blacktop to as high as 0.95 for fresh snow. Representative average values for North America are 0.16 in summer and 0.40 in winter.

Infrared radiation makes a much smaller contribution to the ground energy balance during daylight hours than does solar radiation. At night, however, it increases in significance and plays a role in phenomena such as the formation of frost while air temperature remains above freezing. Sky radiation data are not as generally available as solar radiation data. Consequently, R_{sky} was computed by using Ångstrom's empirical correlation:[23]

$$R_{sky} = \varepsilon_{sky} \sigma T_{db}^4 [a - b \cdot \exp(-2.3c \cdot e)] \qquad \text{[Eq 7]}$$

The term in square brackets functions as a multiplier on the gray emissive power of the sky evaluated at the ambient dry-bulb temperature (T_{db}). This correction factor depends on the moisture content of the air, indicated by the ambient vapor pressure, e (millibars). Note that sky radiation increases with air moisture content. The infrared emissivity of the sky is effectively unity. Coefficients a, b, and c were assigned Geiger's recommended values of 0.820, 0.250, and 0.094.[24]

Ground surface infrared radiation is given by the Stefan-Boltzmann equation:

$$R_g = \varepsilon_g \sigma T_g^4 \qquad \text{[Eq 8]}$$

where T_g is the ground surface temperature. The infrared emissivity, ε_g, is on the order of 0.9 or greater for most natural surfaces.

Expressions for turbulent convection of sensible and latent heat were taken from the work of Kreith and Sellers[25] and Sellers and Dryden:[26]

$$q_{cs} = \rho_{air} c_{p,air} D_h (T_g - T_{db}) \qquad \text{[Eq 9]}$$

---

[22]W. D. Sellers.
[23]R. Geiger, *The Climate Near the Ground* (Harvard University Press, 1961).
[24]R. Geiger.
[25]F. Kreith and W. D. Sellers.
[26]W. D. Sellers and P. S. Dryden, *An Investigation of Heat Transfer From Bare Soil*, Final Reports, Grant No. DA-AMC-28-043-66-G27 (University of Arizona, April 1967).

and:

$$q_{cl} = \rho_{air}\, c_{p,\,air}\, D_w (T_{db} - T_{wb}) \qquad \text{[Eq 10]}$$

where q_{cs} and q_{cl} are the sensible and latent fluxes, D_h and D_w are turbulent transport coefficients for heat and water vapor (m/sec), and T_{wb} is the ambient wet-bulb temperature. Eq. 10 gives "potential" (i. e., maximum) latent loss rather than the actual value. The significance of this substitution is discussed below.

Sellers and Dryden derived D_h and D_w by analogy to D_m, the neutral stability momentum transfer coefficient:

$$D_m = 0.164\, u_{2\,m} \left(\ln \frac{z_w}{z_0} \right)^{-2} \qquad \text{[Eq 11]}$$

where, u_{2m} is the wind speed measured at a height of 2 m, z_w is the wind speed observation height (i.e., 2 m), and z_0 is the "roughness height" of the ground cover. Roughness height may be as small as 1 mm for a very smooth surface or larger than 2 m for a forested surface.[27] While z_0 frequently is on the order of the actual height of ground cover, the relationship is not as direct as the name "roughness height" implies. Because z_0 is defined merely to be the z-intercept of the velocity profile (i.e., the theoretical height at which an experimentally measured velocity profile goes to zero), it is quite possible to obtain negative values of roughness height from data sets that do not fit the logarithmic boundary layer model very well.

To extend the analogy to nonneutral conditions, Sellers and Dryden modified the neutral stability expressions with corrections that depend on the atmospheric temperature gradient at the ground. The corrected expressions are:

$$D_h = \begin{cases} D_m \left[1 + 14 \left(\dfrac{T_g - T_{db}}{u_{2\,m}^2} \right) \right]^{\frac{1}{3}} & \text{if } T_g \geq T_{db} \\ D_m \left[1 - 14 \left(\dfrac{T_g - T_{db}}{u_{2\,m}^2} \right) \right]^{-\frac{1}{3}} & \text{if } T_g < T_{db} \end{cases} \qquad \text{[Eq 12]}$$

[27] W. D. Sellers.

and:

$$D_w = \begin{cases} D_m \left[1 + 10.5 \left(\dfrac{T_g - T_{db}}{u_{2m}^2} \right) \right]^{\frac{1}{3}} & \text{if } T_g \geq T_{db} \\ D_m \left[1 - 10.5 \left(\dfrac{T_g - T_{db}}{u_{2m}^2} \right) \right]^{-\frac{1}{3}} & \text{if } T_g < T_{db} \end{cases} \qquad \text{[Eq 13]}$$

The term q_{et} in Eq 4 comprises all processes at the the surface of the ground that involve exchanges of latent heat. These processes include convection of latent heat (Eq 10), evaporative conversion of sensible heat to latent heat, and transpiration of latent heat by vegetation. Limits on evapotranspiration are imposed by the saturation conditions of the ambient air, the mixing efficiency of the boundary layer, and the supply of moisture available to the surface. For analytical purposes, it is useful to distinguish between evapotranspiration that is limited by the supply of moisture and that which is not. The latter case is referred to as the "potential evapotranspiration regime." It is the theoretical maximum rate for a surface and is limited solely by meteorological conditions. An actual evapotranspiration model requires knowledge about the degree of saturation at the ground surface and could not be used in this study because the soil moisture distribution was not modeled.

Although it is a limiting case, potential evapotranspiration is approximated in some naturally occurring situations--most often through the action of vegetation. Grasses and similar ground cover, when well watered, transpire moisture into the atmosphere at near the potential rate even when the ground surface is relatively dry. The potential evapotranspiration model is thus of wider applicability than its definition suggests. Also, the zero and potential evapotranspiration cases bracket the range of boundary latent heat effects. Because it is sometimes a good model of actual conditions, does not require specification of moisture conditions at the surface, and is a useful asymptotic case, potential evapotranspiration was assumed in the present model.

Expressions for potential evapotranspiration have been derived elsewhere.[28] The working equation given by Sellers is:[29]

$$q_{et} = \left[\frac{\Delta}{\Delta + \gamma} \right] (R_t - G) + \rho_{air}\, c_{p,\,air}\, D_w (T_{db} - T_{wb}) \qquad \text{[Eq 14]}$$

The first term on the right-hand side of Eq 14 represents sensible heat transferred to the surface by radiation or conduction that is converted to latent heat. The dimensionless group $[\Delta/(\Delta+\gamma)]$ is a physical property of air that is tabulated in Jensen.[30] It represents the fraction of a unit of sensible heat transferred to a saturated surface that is converted into latent heat. Parameter Δ is the change in

---

[28] W. D. Sellers; M. E. Jensen (Ed.), *Consumptive Use of Water and Irrigation Water Requirements (American Society of Civil Engineers [ASCE], 1973).*

[29] W. D. Sellers.

[30] M. E. Jensen (Ed.)

saturation vapor pressure with temperature and z is the "psychrometer constant" (the change in vapor pressure per unit temperature difference during an adiabatic saturation process). The second term represents convection of latent heat.

The final form of the surface boundary condition is obtained by substituting from Eqs 6 through 9 and 14 into Eq 3:

$$
\begin{aligned}
G = -k\frac{\partial T}{\partial z} = {} & (1-\alpha_{sol})R_{sol,i} \\
& + \varepsilon_{sky}\sigma T_{db}^{4}\left[a - b\cdot\exp(-2.3\,c\cdot e)\right] - \varepsilon_{g}\sigma T_{g}^{4} \\
& - \rho_{air}\,c_{p,air}\,D_{h}(T_{g}-T_{db}) \\
& - \left[\frac{\Delta}{\Delta+\gamma}\right](R_{i}-G) - \rho_{air}\,c_{p,air}\,D_{w}(T_{db}-T_{wb})
\end{aligned}
\qquad \text{[Eq 15]}
$$

Numerical Solution

The mathematical model of earth-coupled heat transfer described in the preceding section was solved numerically for the case of a three-dimensional slab-on-grade floor by an explicit Patankar-Spalding finite difference formulation.[31] The program was written in FORTRAN 77 and implemented on a VAX 11-785 minicomputer. Details of the numerical solution technique, a sample input form, and a listing of the program can be found in a separate publication.[32]

Execution time for the program ranged from slightly less than 4 hr to as long as 52 hr (on a dedicated machine). Runs at the high end of this range were those with no planes of symmetry available to reduce the size of the computational domain. These were L-shaped floor plans and simulations, including the effect of the building shadow. For symmetrical cases such as unshaded rectangles, it was necessary to model only one-quarter of the domain, thus reducing the number of operations per time step by nearly 75 percent. Typically, five to seven annual cycles were required to achieve a converged periodic temperature distribution throughout the domain. Longer runs occurred in deeper domains and with zero flux lower boundary conditions.

Simulation Parameters

Parameters of the detailed model that could be varied included climate (i.e., the weather file), soil properties, ground surface conditions, and building characteristics such as shape, size, and insulation treatment. Values of these parameters were chosen to span typical ranges that might be encountered in the United States. The following paragraphs describe the model parameters and give the values used in developing the data base for this study.

Climate

Four TMY weather locations were selected to represent the range of climates found in the continental United States. Table 1 lists geographic and climatic data for these sites. Minneapolis and

---

[31]S. V. Patankar, *Numerical Heat Transfer and Fluid Flow* (Hemisphere, 1980).
[32]W. P. Bahnfleth.

Table 1

Test Site Geographic and Climatic Data

Parameter*	Medford, OR	Minneapolis, MN	Philadelphia, PA	Phoenix, AZ
Latitude	42° 2′	44° 5′	[illegible]° 5′	33° 3′
Longitude	122° 5′	93° 1′	[illegible]° 2′	112° 0′
Elevation (m)	396	251	[illegible]	340
T_{mean} (C)	11.7	7.0	12.2	21.9
HDD (C)	2735	4636	2855	77[illegible]
CDD (C)	315	506	614	2023

*T_{mean} = annual mean air temperature, HDD = heating degree days, CDD = cooling degree days.

Phoenix are typical of the cold and hot extremes of U.S. weather. Philadelphia and Medford are situated in moderate climate zones having similar mean temperatures, but different degree days. Oregon's coastal climate is responsible for the less severe conditions observed in Medford. Three of these sites, Medford, Minneapolis, and Phoenix, are located in regions identified by Labs as being well suited for earth-sheltered construction.[33]

Soil Properties

Soil properties were chosen to represent the range of naturally occurring conditions. Data gathered by Kersten,[34] as presented graphically by Andersland and Anderson,[35] were the primary source of guidance for property selection. A mid-range set of properties corresponding to a moist soil was used as the base case in most of the simulations. Four other sets representative of both drier (lower conductivity) and wetter (higher conductivity) extremes were used in a parametric study of property effects. These five sets of properties are shown in Table 2. Properties were varied from one set to another in such a way that thermal conductivity and thermal diffusivity effects could be compared independently. (In set A, for example, "α" remains constant while "k" doubles with respect to the base case. Diffusivity is halved with respect to the base case while conductivity remains constant in set B.) Density and specific heat always appear as a product in this analysis, so they were assigned equal values purely for convenience.

Ground Surface Properties

Ground surface properties were taken from sources summarized by Sellers.[36] A surface ordinarily covered by short grass was assumed. Average solar albedo values were taken from the extensive

[33] K. Labs, "Regional Analysis of Ground and Above-Ground Climate," *Underground Space*, Vol 6, No. 6 and Vol 7, No. 1 (1982).

[34] M. S. Kersten, *Thermal Properties of Soils*, Bulletin No. 28, Vol LII, No. 21 (University of Minnesota Institute of Technology Engineering Experiment Station, June 1, 1949).

[35] O. B. Andersland and D. M. Anderson, *Geotechnical Engineering for Cold Regions* (McGraw-Hill, 1978).

[36] W. D. Sellers.

Table 2

Soil Property Sets

Property*	Base Case	A	B	C	D
k (W/m-K)	1.0	2.0	1.0	0.5	2.0
ρ (kg/m^3)	1200	1700	1700	1200	1500
c (J/Kg-K)	1200	1700	1700	1200	1500
α (m^2/s)	5.9 x 10^{-7}	6.9 x 10^{-7}	3.5 x 10^{-7}	3.5 x 10^{-7}	8.9 x 10^{-7}

* k = conductivity, ρ = density, c = specific heat, α = thermal diffusivity

measurements of Kung et al. who compiled tables of continental averages as a function of latitude and snow cover on the basis of optical measurements taken from an airplane.[37] Values used in this study were:

- 30-35 Degrees North Latitude (Phoenix)--Snow: 0.191, No Snow: 0.172
- 35-40 Degrees North Latitude (Philadelphia)--0.285/0.165
- 40-45 Degrees North Latitude (Medford, Minneapolis)--0.379/0.158.

Data reported by Geiger[38] and others indicate that infrared emissivity is 0.90 or higher for most natural surfaces, including snow and grass. Accordingly, a value of 0.90 was used in all runs. Surface roughness height values of 0.75 cm for short, bare grass and 0.03 cm for snow were used in the convection model.

Building Parameters

Several floor parameters were held constant throughout this study so attention could be focused on the central question of size and shape. Consequently, issues such as details of floor construction, material property differences, and floor coverings were not considered. All floors were 10-cm-thick concrete slabs. Thermal properties of concrete were those given in the *1989 ASHRAE Handbook of Fundamentals*: 0.93 W/m-K, 2300 kg/m^3, and 653 J/kg-K, respectively, for conductivity, density, and specific heat. Insulation, when specified, was polystyrene board with a thermal conductivity of 0.029 W/m-K (i.e., a thermal resistance of 34.5 m-K/W). As noted previously, floor surface conductances of 9.26 W/m^2 and 6.13 W/m^2 were used for heat transfer to and from the room, respectively.

Rectangular and L-shaped floors covering a large range of size and aspect ratio were considered. Values of area varied from a minimum of 144 m^2 to a maximum of 3600 m^2. For most runs, either

[37] E. C. Kung, R. A. Bruison, and D. H. Lenschow, "A Study of Continental Surface Albedo on the Basis of Flight Measurements and Structure of the Earth's Surface Cover Over North America," *Monthly Weather Review*, Vol 92, No. 12 (1964).
[38] R. Geiger.

a "residential" size of 144 m^2 or a "commercial" size of 2025 m^2 was used. Aspect ratio varied from unity (for a square floor) to nine (180 m by 20 m rectangle). Area-to-perimeter ratios ran from 2.4 m to 15 m. Four cases of insulation were considered: 2.54 cm on the slab edge and under the first meter of the floor, 2.54 cm covering the entire outer surface of the slab, and 5.08 cm in both of the preceding configurations.

Parametric Groups

The 93 simulations that form the basis of this study are catalogued in the Appendix. They are grouped into seven series that isolate various effects of interest:

- Series G: floor shape and size/domain depth
- Series W: climate
- Series E: no evapotranspiration
- Series S: shadowing of the ground by the building
- Series K: soil thermal property effects
- Series Z: zero-flux deep ground boundary condition
- Series I: insulation.

The ground surface boundary condition included potential evapotranspiration except in series E and as otherwise noted in the Appendix. All floors other than those in series I were uninsulated. The deep ground boundary condition in all series except Z was a specified temperature condition equal to the annual average air temperature at a depth of either 10 or 15 m (again, as indicated in the Appendix). In each series, several area and aspect ratio combinations were considered to show how the effect produced by the parameter under study depended on geometric factors.

3 CHARACTERISTIC LENGTH METHOD

This chapter describes a procedure for estimating whole-floor heat transfer rates from a slab-on-grade that is suitable for use either as a manual method or in simple computer models. A portion of the data from the finite difference model are referenced in this discussion, however, not all of the parametric studies listed in the preceding chapter are described here. The interested reader should consult USACERL Technical Manuscript (TM) E-89/11 for a complete exposition of parametric study results. Presentation of the proposed method is prefaced by a discussion of the method currently recommended by ASHRAE for design heat loss calculations. This discussion serves to identify the shortcomings of existing models that motivate the development of an improved method. A more detailed qualitative consideration of floor heat loss characteristics can be found in TM E-89/11.

Overview

The well known 1948 study by Bareither et al. used 3 months of heating season measurements to evaluate two simple models of unheated slab floor heat loss:[39]

$$Q = F_1 \cdot P \cdot \left(T_{inside} - T_{outside} \right) + 2 \cdot A_{inside} \qquad \text{[Eq 16]}$$

and:

$$Q = F_2 \cdot P \cdot \left(T_{inside} - T_{outside} \right) \qquad \text{[Eq 17]}$$

where Q is the total rate of floor heat loss in Btu/hr.** Eq 16 distinguishes between heat lost at the slab edge and heat lost to the ground through the "inner area" of the floor (A_{inside}, total floor area less the area of a 2-ft strip around the perimeter). The edge loss is a function of floor perimeter length, P (ft); indoor-outdoor air temperature difference, T_{inside}-$T_{outside}$ (°F); and a construction-dependent perimeter heat loss factor "F_1" [Btu/(hr/sq ft)]. The latter component was found to be approximately 2 Btu/(hr/sq ft) of inner floor area. Eq 17 predicts whole-floor loss on the basis of perimeter length only, using a different set of factors, F_2. Both methods relate floor heat loss to the instantaneous indoor-outdoor temperature difference.

Bareither et al. concluded that the F_1 method is the more accurate of the two. The F_2 method, however, was judged to be adequate for area-to-perimeter (A/P) ratios of 12 ft or less. For larger values of A/P, the neglected loss from the inner area caused large errors. These researchers' recognition of the need to account for heat transfer from the "core" or "inner" floor area of medium-to-large buildings is an important observation that is generally neglected by designers today. It is widely presumed that the large perimeter heat loss rates common during the heating season render the much smaller core flux irrelevant to the total floor heat loss rate. The *1989 ASHRAE Handbook of Fundamentals* recommends the F_2 method with no caveats concerning the limits of its applicability.

---

[39]H. D. Bareither, A. N. Fleming, and B. E. Alberty.

**These equations do not use metric units: conversion factors are: 1 Btu = 3.412 w, 1 ft = 0.305 m, 1 sq ft = 0.092m^2, °F = (°C x 1.8) + 32.

The numerical results plotted in Figure 2 challenge the fundamental premise of the F_2 method that floor heat loss is proportional to perimeter length. The figure compares heat loss per unit of perimeter for 12 by 12 m and 45 by 45 m slabs in Medford, OR. The two curves are similar in shape, but

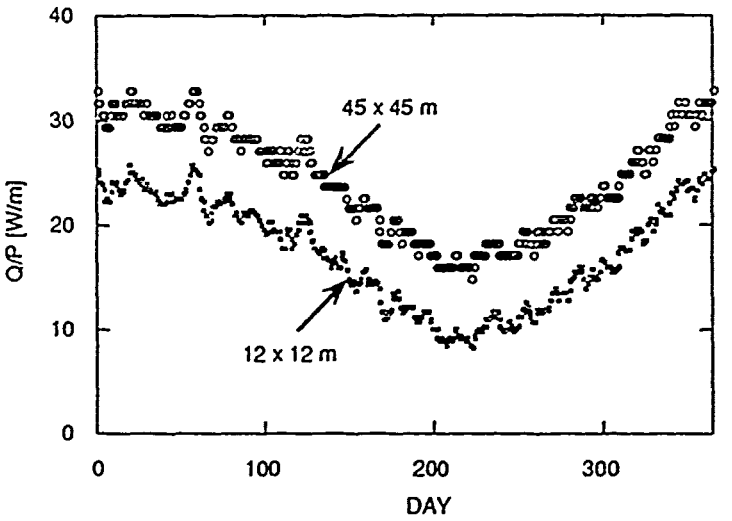

Figure 2. Daily-averaged heat loss per unit perimeter length for large and small slabs, Medford, OR.

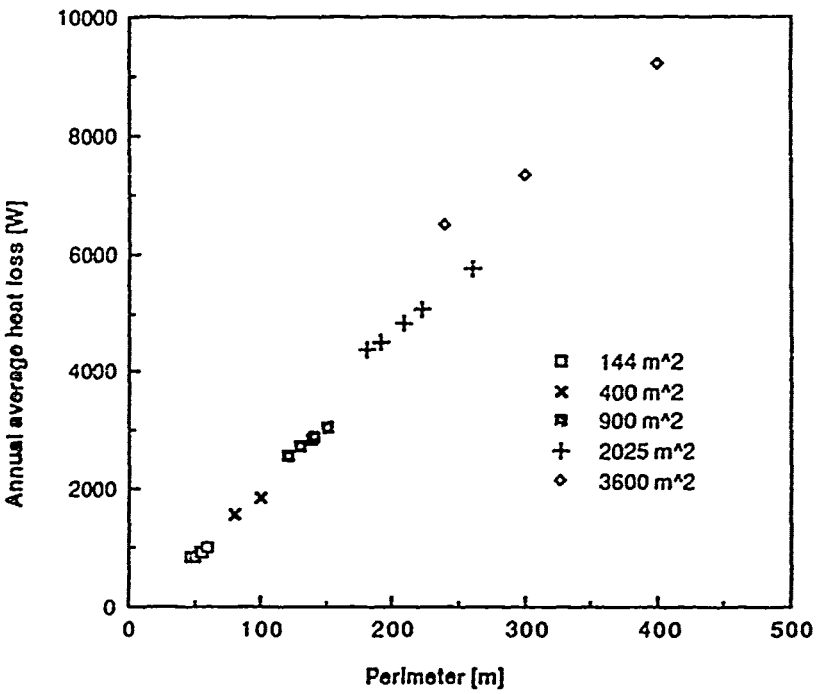

Figure 3. Heat loss vs. perimeter length for uninsulated floors in Medford, OR (15-m-deep domain).

offset from one another by approximately 8 W/m over the entire year due to the greater core loss per perimeter unit of the larger building. This example indicates the important role played by core losses in larger buildings and the considerable error that can be introduced by the use of F_2 coefficients based on small building data. Heat loss estimates for the 45 by 45 m floor extrapolated from the flux per unit perimeter length of the 12 by 12 m floor would be low by roughly 25 percent in the winter and 50 percent in the summer for this case.

Several features of the heat loss distributions in Figure 2 are relevant to possible modeling strategies. Although fluctuations with a period of 1 week or less are evident, the predominant pattern is a single annual cycle of approximately sinusoidal shape. On a relatively short time scale, i.e., periods of less than 1 week, both floors experience heat loss fluctuations of about the same magnitude per unit of perimeter because the heat loss profile near the edge is not very sensitive to floor area. The difference between the two cases, therefore, is a difference of mean heat loss. This suggests that mean and fluctuating components of heat loss should be distinguished in a model.

Model Description

Shape and Size Effects on Mean Heat Flux

Since it is clear that the fundamental geometric hypothesis of the F_2 method can cause large errors in floor heat transfer estimates, an improved scaling relationship is an essential element to an accurate model. Data from the series G runs were studied to determine the relationship between shape, size, and heat transfer rate. Constant factors in these runs were Medford weather, base case soil properties, potential evapotranspiration surface condition, and a lower boundary temperature fixed at the annual average dry bulb. Area varied from 144 to 3600 m^2 and area/perimeter varied from 2.4 to 15 m. Plan shape was rectangular with the exception of three L-shaped cases (areas of 144, 900 and 2025 m^2).

Figure 2 gives evidence that effects of area on heat loss are localized in the mean component. The area effect on mean loss is shown even more clearly in Figure 3, which gives annual average heat loss as a function of perimeter for 20 series G runs with a 15-m-deep domain. Five floor areas and a variety of aspect ratios are represented. For a given perimeter length, there is a significant area effect on average loss. Heat transfer data from a given floor describe a curve that would lie above curves corresponding to smaller areas and below those corresponding to larger areas. L-shaped floors fall into place among rectangles of the same area in Figure 3 (for example, the middle point of the five 2025 m^2 cases is an L-shaped slab). The relationship between area and perimeter--not the particular shape--seems more important. The presumed independence of shape should not be taken to extremes, however. It is easy to imagine multiply connected shapes, such as buildings with enclosed courtyards, that might not fit this hypothesis.

On the basis of the observations that (1) mean heat loss is somehow proportional to both perimeter and area and (2) the particular plan shape of a floor is not of great significance, it was decided to develop and test a model of geometric effects based on the length scale A/P, a measure of the narrowest dimension of a planar shape. For a square of side "L", A/P is equal to L/4. In the general case of a rectangle with short side "L" and aspect ratio "μ" (defined ≥ 1), A/P is equal to $L/[2(1+1/\mu]$. Thus, an infinite strip of length "L", which has an aspect ratio of infinity, has an A/P of L/2. When the data of Figure 3 are replotted as annual-averaged heat loss per unit area vs. A/P, the result is Figure 4. All of the data lie on a single curve approximated by the logarithmic function:

$$q = c \cdot \left(\frac{A}{P}\right)^d \qquad \text{[Eq 18]}$$

where c and d are constants. For a given rectangular area, a square has the largest value of A/P, so for each group of data plotted in Figure 4, the square case is the right-most point. Note that there is overlap between the A/P values of the 2025 m^2 and 3600 m^2 data, and that the heat flux values for these overlapping cases fall into place quite well on the same curve. As the characteristic width of a slab increases, its average rate of heat loss decreases. This occurrence reflects the fact that floors with large A/P have proportionately more low-flux "core" area than those with small values of A/P.

The constants c and d depend on a great many parameters, including the annual average temperature difference, soil properties, domain geometry, and details of foundation design. There is no reason to suppose that the value -0.736 for exponent d is universal in any sense. In addition, the fluctuating component of heat transfer appears to behave differently than the mean (refer again to Figure 2). The extension of Eq 18 to include these effects will be considered in subsequent sections.

It is worthwhile to consider the implications of the heat flux relation (Eq 18) for average whole-floor heat loss. The whole-floor heat transfer rate implied by Eq 18 is:

$$Q = c \cdot \left(\frac{A}{P}\right)^{d} \cdot A = c \cdot P^{-d} \cdot A^{1+d} \qquad \text{[Eq 19]}$$

If d has a value of -1, then Eq 19 is independent of area and is a linear function of perimeter. Values of d greater than -1 indicate a combined dependence on total area and perimeter. A value of 0 would indicate linear dependence on area and independence of perimeter. If d is greater than 0, Eq 19 implies that an increase in perimeter would lead to decreased heat loss for a fixed area. A value of d less than -1 implies that heat loss decreases as area increases. Both of these behaviors are implausible. Therefore, on physical grounds, it seems that values of d must lie between these limiting cases of 0 and -1.

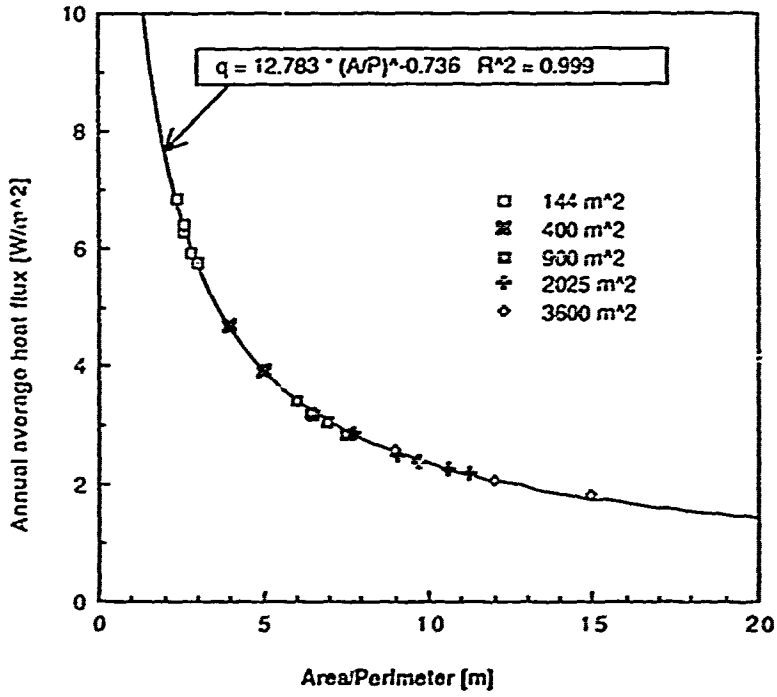

Figure 4. Heat loss per unit area vs. A/P for uninsulated slabs, Medford, OR (15-m-deep domain).

Extension of Model to Transient Heat Flux

The mean heat flux model presented in the preceding section can be extended into a method for approximating the daily averaged transient heat loss. Linear conduction theory permits the decomposition of the total floor heat flux into mean and fluctuating parts:

$$q_{total}(t) = q_{mean} + q_{periodic}\ (t) \qquad \text{[Eq 20]}$$

If it is assumed that the mean heat loss is proportional to the difference between the indoor air and outdoor ground surface temperatures and that the periodic loss is a function of the difference between the daily averaged and annual mean ground surface temperatures, then for a given floor:

$$q_{total}(t) = K_1 \cdot \left(T_{room} - T_{g,\,mean}\right) + K_2 \cdot \left(T_{g,\,mean} - T_{g,\,\phi}\right) \qquad \text{[Eq 21]}$$

where K_1 and K_2 are constant mean and periodic conductances (SI units W/m^2-K) and $T_{g,\phi}$ is the time-dependent, phase-lagged ground surface temperature. Ground surface temperature was chosen as an ambient condition because it directly represents conditions in the soil--which may be much different from air temperature. (This point is discussed in more detail below.) The phase lag "ϕ" accounts for shifting of floor heat transfer by the mass of soil thermally attached to it.

The ground temperature, T_g, can be approximated by a sinusoidal least squares model of soil temperature data. In this study, numerical surface temperature predictions served as the raw data approximated by Eq 22:

$$T_g = T_{g,\,mean} + \Delta T_g \cdot \sin\left(2\pi \frac{(Day + \zeta)}{365}\right) \qquad \text{[Eq 22]}$$

where ΔT_g is the amplitude of the annual ground temperature cycle, "Day" is the day of the year (1 through 365), and ζ is the shift (in days) of the ground temperature with respect to the calendar. $T_{g,\phi}$ differs from T_g only by virtue of the additional phase shift, ϕ:

$$T_{g,\,\phi} = T_{g,\,mean} + \Delta T_g \cdot \sin\left(2\pi \frac{(Day + \zeta + \phi)}{365}\right) \qquad \text{[Eq 23]}$$

The scaling approach of Eq 18 is used to model the geometry dependence of K_1 and K_2 for arbitrary floors. Each conductance is presumed to vary independently of the other, so each is equated with an expression of the same form as Eq 18:

$$K_1 = c_1 \cdot \left(\frac{A}{P}\right)^{d_1} \qquad \text{[Eq 24]}$$

and:

$$K_2 = c_2 \cdot \left(\frac{A}{P}\right)^{d_2} \qquad \text{[Eq 25]}$$

Note that Eqs 24 and 25 presume K_1 and K_2 to vary independently. With substitution from Eqs 23 through 25, the complete daily averaged heat flux model of Eq 21 becomes:

$$q_{total}(t) = c_1 \cdot \left(\frac{A}{P}\right)^{d_1} \cdot \left(T_{room} - T_{g,\,mean}\right)$$

$$- c_2 \cdot \left(\frac{A}{P}\right)^{d_2} \cdot \Delta T_g \cdot \sin\left(2\pi \frac{(Day + \zeta + \phi)}{365}\right) \qquad \text{[Eq 26]}$$

Values of the constants c_1, c_2, d_1, and d_2 are determined by a two-stage process. First, K_1 and K_2 values are calculated for several floor A/P values by least squares approximation of daily averaged heat flux results. Then, c_1, c_2, d_1, and d_2 are obtained by a second series of approximations using Eqs 24 and 25. The phase lag, ϕ, has been found to vary little over a range of floor sizes; therefore, it seems acceptable to use an average value in Eq 23.

Numerical ground temperature results and the sinusoidal least squares ground temperature approximation T_g for the Medford, OR cases of Figures 3 and 4 are shown in Figure 5 (a). Daily averaged heat flux results and the approximate model q_{total} for the 12 by 12 m uninsulated slab appear in Figure 5 (b). Ground surface temperatures show much more scatter with respect to T_g than do heat flux results with respect to q_{total}. The relatively smoother heat flux data reflect the damping effect of soil thermal mass. The phase lag ϕ causes an offset between the day of peak heat loss and the day of minimum ground surface temperature of approximately 18 days.

Table 3 gives model coefficients for four representative uninsulated floors in Medford, OR. Values of K_1 and K_2 decrease with increasing A/P. In contrast, phase lag increases slightly (by approximately 1 day) as area increase from 144 m^2 to 2025 m^2, but decreases as A/P increases for a given area. Values of c_1, c_2, d_1, and d_2 derived from these four cases are, respectively, 0.978, 0.713, -0.747, and -0.999. The values of c_1 and d_1, which pertain to the annual average component of heat loss, agree very well with the values of c and d (Eq 18) computed for the entire Medford data set and shown in Figure 4. Exponents d_1 and d_2 differ by only 1.5 percent of their mean value. The product of c_1 and the average indoor to ground surface temperature difference is similarly close to analogous constant c (13.105 vs. 12.783). The good agreement between coefficients derived from both large and small sets of results is encouraging evidence that the scaling approach of Eq 18 has physical significance. Floor area seems to affect only the mean heat transfer rate. The value of d_2 differs from the area independent limit of -1 by less than 0.01 percent. Thus, the periodic component of heat loss is a nearly linear function of perimeter and essentially independent of area.

The effect of domain depth (z_{max}) was investigated by comparing results for z_{max} = 10 m with the z_{max} = 15 m Medford results considered previously. In all cases, the annual average heat loss was greater for z_{max} = 10 m, but the magnitude of the difference depended on A/P. Table 4 compares the annual average heat loss for several floors as a function of z_{max}. For the smallest area, 144 m^2, there is no appreciable difference between the two cases. As area (and more particularly, A/P) increase, differences become larger. An explanation consistent with these results is that the strength of interaction between a floor and a lower boundary surface is related to the comparative magnitudes of A/P and z_{max}. A building with small A/P creates a temperature disturbance that does not penetrate very deeply into the ground. As size increases, the boundaries of the building-induced disturbance expand and the building's heat loss becomes sensitive to changes in conditions at greater and greater distances. In this sense, a boundary is "deep" only if it satisfies the twin criteria of being beyond the annual penetration depth of the soil temperature distribution *and* deeper than the length scale of the building in question.

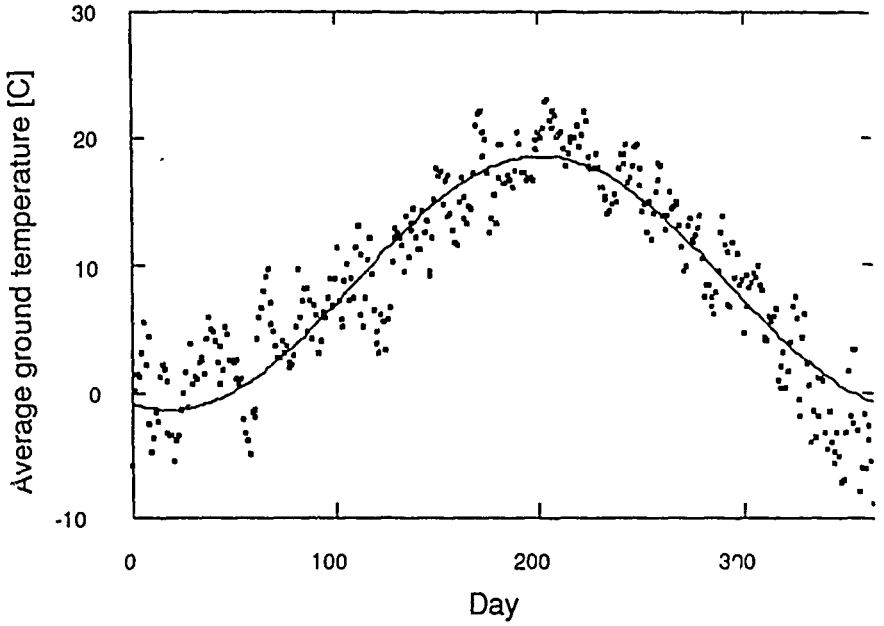

(a)

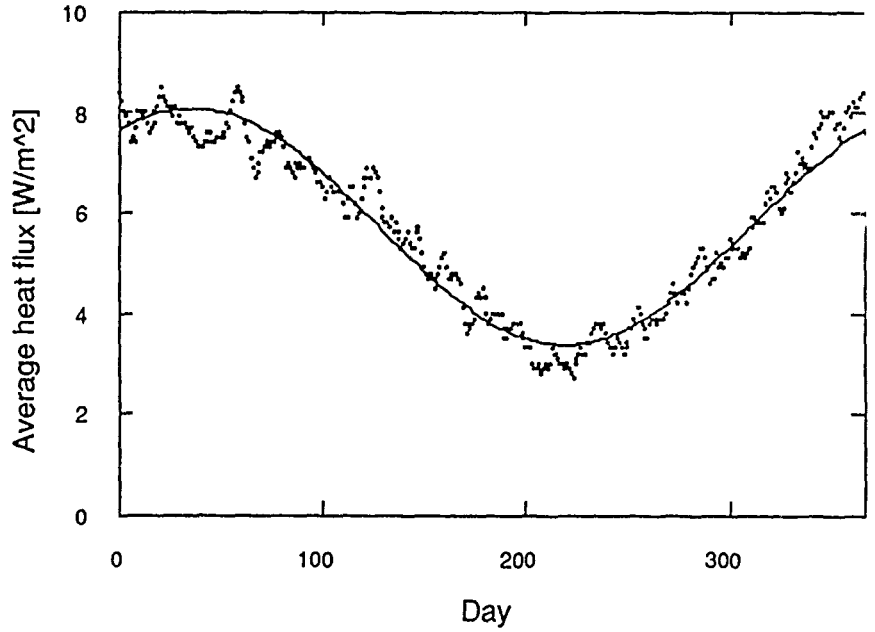

(b)

Figure 5. Daily-averaged heat loss model for a 12 by 12 m floor in Medford, OR: (a) average ground surface temperature (b) average heat flux.

Table 3

Daily Average Heat Loss Model Coefficients for Medford, OR
(15-m-Deep-Domain)

Run ID	Dimensions (m)	Area (m^2)	A/P (m)	K_1(W/m^2)	K_2(W/m^2)	ϕ (days)
GR04	6 x 24	144	2.4	0.510	0.299	-17.885
GR1A	12 x 12	144	3.0	0.428	0.236	-17.811
GR8A	18 x 112	2016	7.75	0.212	0.093	-17.812
GR5B	45 x 45	2025	11.25	0.161	0.064	-18.381

Climate Effects

Performance of the proposed model was tested with simulation results from four climates: Medford, OR; Minneapolis, MN; Philadelphia, PA; and Phoenix, AZ. Medford results were taken from series G. The other cases are grouped as series W in the Appendix. All had potential evapotranspiration ground surface conditions fixed temperature lower boundary conditions at a depth of 15 m. Following the approach of the previous section, least squares models of daily averaged heat flux were computed and model coefficients were compared.

Table 5 contains the parameters of sinusoidal least squares models for air and ground temperature in each location. Note the varying degrees of difference between ground surface and air temperature for the four sites. For the three temperate cases--Medford, Minneapolis, and Philadelphia--the mean ground temperature is depressed from 2.4 to 2.9 °C beneath the average dry bulb and the amplitude* of the daily average ground temperature is within a degree of the air temperature amplitude. For Phoenix, however, which has a warm, dry climate with year-round high evapotranspiration potential, the mean ground temperature is a full 6 °C less than mean air temperature and the ground temperature model amplitude is 3.4 °C smaller than the dry-bulb amplitude.

These results demonstrate that air temperature may not be a reliable indicator of ground temperature when accuracy is important. Because mean losses depend on relatively small temperature differences, large uncertainty is introduced by using the indoor/outdoor air temperature difference as the reference for floor heat loss. Figure 6 compares air and ground temperature models for Phoenix, AZ, the case of worst agreement. Note that the two differ by as much as 10 °C during mid-summer.

Table 6 gives K_1, K_2, and ϕ values for the Minneapolis, Philadelphia, and Phoenix series W runs. The corresponding results for Medford were tabulated previously in Table 3. Case-by-case comparison of K_1 and K_2 shows that the models for Medford, Minneapolis, and Philadelphia are quite consistent with one another. The spread among these three sites is within about 10 percent of the mean. Because these model coefficients are similar, it is reasonable to conclude that differences in climate are

*Values of amplitude in Table 5 are negative as a result of the form of the model and the choice of representation for phase shift. Only the magnitude is of significance to this discussion.

represented appropriately by differences in the annual mean and amplitude of ground temperature.* K_2 values for Phoenix are in good agreement with the other three sites, but values of K_1 are significantly lower. It is possible that the proposed model is subject to error or behaves nonlinearly when the mean indoor and outdoor temperatures are comparable (i.e., when their difference becomes small) as is the case for Phoenix.

Table 4

Effect of Lower Boundary Depth on Mean Heat Loss for Uninsulated Floors in Medford, OR

Dimensions (m)	Area (m^2)	A/P (m)	$Q_{15\,m}$ (W)	$Q_{10\,m}$ (W)	Δ%
12 x 12	144	3.0	822.97	825.69	0.33
15 x 60	900	6.0	3062.71	3142.60	2.61
30 x 30	900	7.5	2583.86	2702.96	4.61
23 x 88	2024	9.1	5076.08	5386.06	6.11
45 x 45	2025	11.25	4367.89	4760.13	8.98
30 x 120	3600	12.0	7319.34	8001.86	9.32
60 x 60	3600	15.0	6467.18	7281.86	12.60

Table 5

Mean, Amplitude, and Phase Shift for Models of Daily Averaged Air and Ground Surface Temperatures

Location	$T_{air,\,mean}$ (C)	ΔT_{air} (C)	ζ_{air} (days)	$T_{g,\,mean}$ (C)	ΔT_g (C)	ζ_g (days)
Medford, OR	11.4	-9.7	69.2	8.6	-9.9	73.0
Minneapolis, MN	7.2	-17.0	72.3	4.8	-16.3	72.6
Philadelphia, PA	12.4	-12.6	68.9	9.5	-12.1	68.8
Phoenix, AZ	21.9	-11.7	72.2	15.9	-8.3	68.3

*Bear in mind, however, that more subtle effects of climate variation are not explicitly incorporated in this model. For instance, the effect of evaporative heat transfer is greatest in warm weather and practically vanishes during cold weather. Consequently (as will be shown in a subsequent section), evapotranspiration may be relatively uniform over the entire year in a warm climate such as Phoenix and quite seasonal in a cold climate similar to Minneapolis. In the present case, this effect is apparent only in differing ground temperatures recorded in Table 5.

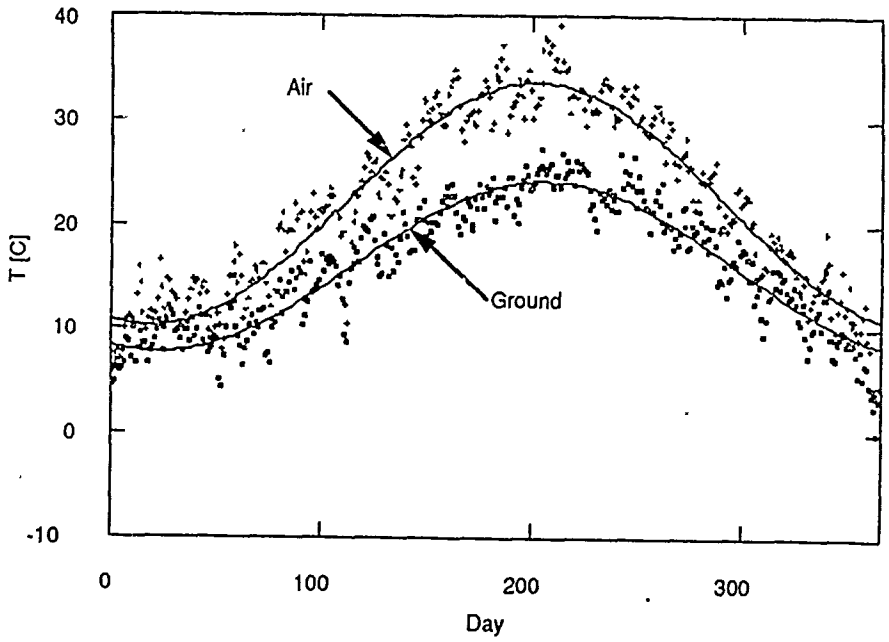

Figure 6. Daily averaged air and ground surface temperatures for Phoenix, AZ (potential evapotranspiration).

Table 7 gives coefficients of daily averaged heat flux models for arbitrary A/P derived from the data of Table 6. These data also show the strong similarity between results for Medford, Minneapolis, and Philadelphia. In all four locations, the time-varying component of heat loss was linearly proportional to perimeter length and independent of area ($d_2 \approx -1.0$). The primary difference between Phoenix and the other sites is in the degree of area dependence of the steady-state heat transfer component (much weaker for Phoenix). It may be that d_1 was larger for Phoenix because the deep ground and indoor temperatures were nearly identical in this case. When there is no mean temperature difference between the floor and the deep ground, any mean loss must be toward the ground surface from the floor perimeter. In this limit, the mean loss should depend on perimeter in a manner similar to the periodic loss.

Values of K_1 and K_2 obtained relative to an air temperature reference showed a systematic variation with annual average temperature from one climate to another. Values obtained with a ground temperature reference were more nearly independent of climatic changes. The cause of strong climate dependence in the former case is the increase in fractional error due to the presumed equivalence of air and ground temperatures as these values approach the reference indoor temperature. For example, if the indoor setpoint is 22 °C, the outdoor air mean is 7.2 °C, and the mean ground temperature is 4.8 °C (as in Minneapolis), then the ratio of the mean indoor/outdoor air temperature difference to the mean indoor/ground surface temperature difference is (22 - 7.2)/(22 - 4.8) = 0.86. The two differ by only 14 percent. In Phoenix, however, where the mean air and ground temperatures were, respectively, 21.9 and 15.9 °C, the corresponding ratio of temperature differences was 0.016. In this case, the indoor/outdoor air temperature difference is nearly two orders of magnitude smaller than the mean difference actually imposed on the floor. When the air reference temperature differs from the "actual" temperature difference, K_1 must change by an amount proportional to the error in order to obtain the correct mean heat loss. As this example shows, that correction would be much larger for Phoenix than for Minneapolis, so K_1 and K_2 would lose their independence of climate. The obvious way to avoid this problem is to adopt a ground temperature reference.

The importance of allowing for surface temperatures that deviate from air temperature is further shown by the results of the parametric study of zero-evaporation surface conditions in TM E-89/11.[40] These results indicated a possible difference in floor heat transfer rates of 20 to 30 percent in temperate climates as a result of differences in ground surface conditions.

Table 6

Daily Heat Loss Model Coefficients for Climate Variation Tests (Case by Case)

a) Minneapolis, MN

Run ID	Dimensions (m)	Area (m^2)	A/P (m)	K_1 (W/m^2)	K_2 (W/m^2)	ϕ (days)
WMN3	6 x 24	144	2.4	0.527	0.318	-16.503
WMN1	12 x 12	144	3.0	0.440	0.251	-16.467
WMN4	18 x 112	2016	7.75	0.221	0.099	-17.226
WMN2	45 x 45	2025	11.25	0.170	0.068	-17.413

b) Philadelphia, PA

Run ID	Dimensions (m)	Area (m^2)	A/P (m)	K_1 (W/m^2)	K_2 (W/m^2)	ϕ (days)
WPH3	6 x 24	144	2.4	0.525	0.322	-16.104
WPH1	12 x 12	144	3.0	0.437	0.254	-15.854
WPH4	18 x 112	2016	7.75	0.217	0.101	-16.681
WPH2	45 x 45	2025	11.25	0.165	0.069	-16.822

c) Phoenix, AZ

Run ID	Dimensions (m)	Area (m^2)	A/P (m)	K_1 (W/m^2)	K_2 (W/m^2)	ϕ (days)
WPX3	6 x 24	144	2.4	0.473	0.323	-15.930
WPX1	12 x 12	144	3.0	0.386	0.255	-15.833
WPX4	18 x 112	2016	7.75	0.167	0.101	-16.504
WPX2	45 x 45	2025	11.25	0.115	0.069	-16.722

[40]W. P. Bahnfleth.

Table 7

Daily Averaged Heat Loss Model Coefficients for Climate Variation Tests (Composite)

Location	c_1	d_1	c_2	d_2
Medford, OR	0.978	-0.747	0.713	-0.999
Minneapolis, MN	0.997	-0.735	0.759	-0.999
Philadelphia, PA	1.007	-0.750	0.765	-0.995
Phoenix, AZ	1.041	-0.901	0.769	-0.997

Soil Thermal Property Effects

The proposed model does not have features that explicitly account for variations in soil and building material thermal properties. However, sets of coefficients for a range of soil conditions could be interpolated for application purposes. In series K, four different combinations of soil k and α were applied to uninsulated floors with four values of A/P in Philadelphia weather. The standard boundary conditions used in other series also applied to this group, i.e., potential evapotranspiration at the ground surface and fixed temperature in the deep ground. The series W Philadelphia runs, which had "base case" properties, provided a fifth set of results. These five property groups are listed in Table 2. Property sets were chosen to permit isolation of thermal conductivity and thermal diffusivity effects. Two pairs (base case/B and A/D) have like conductivity but different diffusivity values, and two (base case/A and B/C) have like diffusivity but different conductivity values. In total, three values each of diffusivity and conductivity were considered. Conductivity varied by a factor of two in either direction from the base value. Diffusivity varied from a factor of two smaller to a factor of 1.3 larger than the base value.

The total, daily averaged heat loss results for varied property runs summarized in Table 8 show that conductivity and diffusivity have much different effects on heat loss. The most important influence of thermal conductivity is its role in determining the mean heat loss from a floor. For example, Q_{avg} for the 45 by 45 m floor varies from less than 2500 W to more than 7000 W over a thermal conductivity range from 0.5 to 2.0 W/m-K. Thus, a four-fold increase in thermal conductivity produces a nearly three-fold increase in mean heat loss.

Diffusivity has a negligible effect on the mean value of heat loss because thermal mass is irrelevant to steady-state heat transfer processes. (Thermal diffusivity vanishes from the heat conduction equation in the steady-state case.) For example, consider the difference in mean heat loss between the base and set B property cases for an 18 by 112 m floor. The 20 W discrepancy is less than 0.5 percent of the mean, an insignificant difference for practical purposes. Diffusivity *does* influence the annual range of heat loss. For a given value of conductivity, larger ranges of heat loss correspond to larger diffusivity values. For instance, the difference between Q_{max} and Q_{min} for the property set B ($k = 1$ W/m-K, $\alpha = 3.5 \times 10^{-7}$ m^2/sec) 12 by 12 m floor is 921.6 W. The annual range with base case properties (same conductivity, but a larger diffusivity of 6.9×10^{-7} m^2/sec) is 1036.8 W. An increase of approximately 100 percent in thermal diffusivity causes the annual range to widen by 115.2 W, an increase of only 12.5 percent.

Thermal conductivity, too, affects the amplitude of annual heat loss. Returning to the previous example, if the base case thermal diffusivity is fixed and conductivity is doubled (as in case A), the annual heat loss range increases to 1440.0 W, a change of 518.4 W or 56.3 percent. The greater influence of conductivity shown by these examples indicates that heat loss on a daily averaged scale is quasi-steady with respect to the soil temperature distribution. Figure 7 gives further evidence of the

relative importance of conductivity and diffusivity on the daily scale. Figure 7 (a) shows distance-weighted least squares approximations to the daily averaged unit heat flux of the 12 by 12 m base and set B property groups. There is no significant change in mean heat loss and only a small change in amplitude. In Figure 7 (b), a large shift in mean heat loss is evident when conductivity changes by a factor of two while diffusivity is held constant. The sizable offset between the two curves reduces the difference between the minimum values occurring during the summer and exaggerates the difference in winter maxima. The greatest difference approaches 5 W/m^2, considerably larger than the magnitude of the diffusivity effect in Figure 7 (a).

Table 8

Heat Loss Data for Varied Thermal Property Cases *

Dimensions (m)	Area (m^2)	Properties	Q_{min} (W)	Q_{max} (W)	Q_{avg} (W)
12 x 12	144	Base	302.4	1339.2	784.3
"	"	A	547.2	1987.2	1226.6
"	"	B	345.6	1267.2	781.8
"	"	C	187.2	835.2	482.9
"	"	D	504.0	2030.4	1227.9
6 x 24	144	Base	331.2	1641.6	941.8
"	"	A	576.0	2419.2	1454.0
"	"	B	388.8	1555.2	937.2
"	"	C	201.6	1022.4	584.0
"	"	D	532.8	2476.8	1454.9
45 x 45	2025	Base	2227.5	6277.5	4152.6
"	"	A	4252.5	9922.5	7003.7
"	"	B	2632.5	6075.0	4207.6
"	"	C	1215.0	3847.5	2450.5
"	"	D	4252.5	10125.0	6997.6
18 x 112	2016	Base	2822.4	8467.2	5443.2
"	"	A	5241.6	13305.6	9018.9
"	"	B	3024.0	8064.0	5463.6
"	"	C	1612.8	5040.0	3232.2
"	"	D	5040.0	13507.2	9026.7

Thermal property values also influence the area dependence of floor heat loss. The nature of these effects appears as effects on the coefficients of the proposed model. Figure 8 shows K_1 and K_2 coefficients as a function of A/P for the cases summarized in Table 8. Curves through the plotted values of K_1 and K_2 are instances of Eqs 24 and 25, respectively. Each curve is labeled to show its values of c_1 and d_1 or c_2 and d_2 as appropriate. The observations made above concerning conductivity and diffusivity dependence are readily apparent in these plots.

*Philadelphia, PA weather and potential evapotranspiration.

In Figure 8 (a), K_1 values for cases with the same conductivity but different diffusivities essentially coincide, indicating the absence of a diffusivity effect on mean heat loss. Fractional changes in K_1 are comparable to, but smaller than, corresponding changes in k. The area effect of thermal conductivity on K_1 increases with increasing k. This occurrence is indicated by the decreasing magnitude of d_1 (the exponent of A/P) as k becomes larger. Area dependence increases because heat loss from the low-gradient core region of the floor grows more rapidly than edge loss when k increases, thus weighting total area more heavily. The results presented in Table 9 illustrate this phenomenon. For both 12 by 12 m and 45 by 45 m floors, the floor center heat loss changes almost in direct proportion to the soil conductivity (i.e., if k is reduced by a factor of two, the center flux is halved.) Maximum edge flux values, however, change by 20 percent or less in response to twofold increases and decreases in k. Thus, more of the difference in floor average heat loss results from changes in core loss.

The value of K_1 decreases more rapidly with increasing A/P for lower values of conductivity. Consequently, the fractional change in K_1 due to a given increase in conductivity grows with increasing A/P. The percentage change in mean heat loss resulting from an increase of k from 1 to 2 W/m-K with α fixed at 6.9×10^{-7} (base case vs. set A properties), for a 6 by 24 m slab (A/P = 2.4 m) is 54.4 percent. When A/P increases to 3 m (12 by 12 m square), the fractional change increases to 56.4 percent. Floors with A/P values of 7.75 m (18 by 112 m rectangle) and 11.25 m (45 by 45 m square) experience increases of 65.7 and 68.7 percent, respectively.

Figure 8 (b), which shows K_2 as a function of A/P, confirms other observations made previously. This plot clearly indicates the subordinate role that thermal diffusivity plays to conductivity in the determination of K_2 and consequently, the periodic component of floor heat loss. Note that cases with like conductivity fall much closer together than those with like diffusivity but different conductivities. As in other cases considered previously, K_2 for these varied property groups is essentially proportional to $(A/P)^{-1}$, indicating that the periodic heat loss component is linearly proportional to perimeter length.

Floor heat loss phase lag results are summarized in Figure 9. For the cases considered, ϕ ranged from 2 to 3 weeks. Clearly, soil properties exercise a much stronger influence on phase lag than floor size. Although there is some pattern to the size dependence of these results, a clear relationship such as that deduced for K_1 and K_2 is not apparent. For a given set of properties, ϕ varied by 2 days or less. Lower values of soil conductivity corresponded to less phase lag, and for a given conductivity, an increase in thermal diffusivity of the soil caused ϕ to decrease. Phase lag, like the conductances K_1 and K_2, was more responsive to changes in conductivity than to changes in diffusivity. While the magnitudes of ϕ observed in this study were not particularly large, 2- to 3-week lags are significant because they support an argument against models based on instantaneous indoor/outdoor temperature differences. The floor heat loss on a particular day results from weather events over a prior period of several weeks.

The results of this series of tests clearly show that soil thermal conductivity must be a parameter in any simplified model of slab-on-grade heat loss that purports to be both general and accurate. If k is specified incorrectly, heat loss rates could easily err by a factor of 2. The effect of conductivity on both "c" coefficients of Eq 26 is quite strong. Conductivity also exercises some influence over the exponent d_1, and consequently, on the area dependence of the steady-state heat loss component. Variation in thermal diffusivity, however, does not seem to have much effect on heat loss and probably does not need to be included as an explicit model parameter.

Building parameters such as details of foundation configuration, material properties, insulation, and floor covering all have the potential to change the overall conductance of a floor. The effects of these parameters are confounded with the effect of soil properties in the coefficients of Eqs 21 and 26 and can be separated only by the comparison of parametric sets of simulations. Therefore, a manual method based on Eq 26 must be based on results encompassing not only several soil types, but also

a variety of foundation designs. The utility of constructing such a method would depend to a great extent on the importance of foundation losses in the intended application and the expense incurred to acquire and validate the necessary base of numerical results.

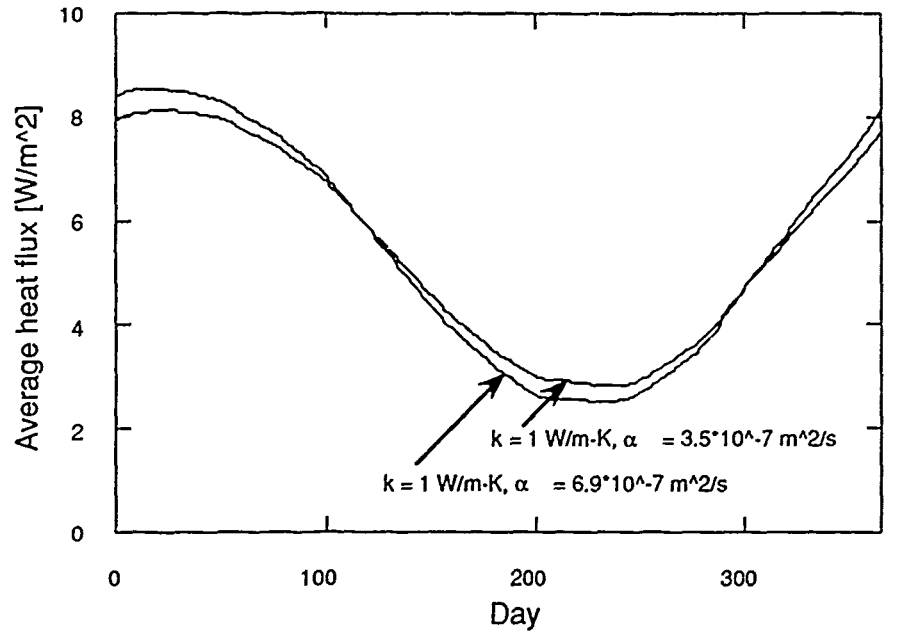

(a) α varied

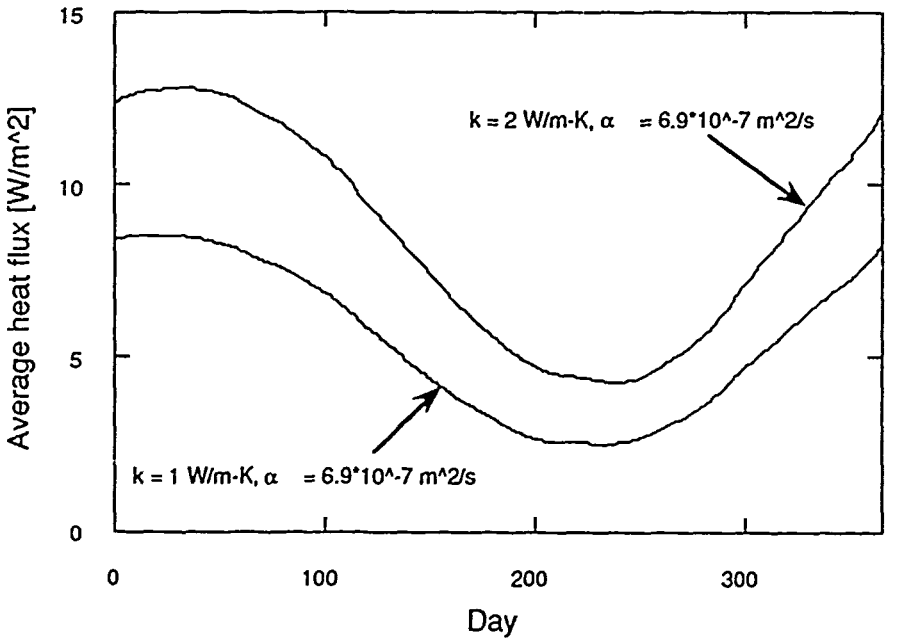

(b) k varied

Figure 7. Typical effects of k and α variation on smoothed, daily-averaged heat loss from a 12 by 12 m floor.

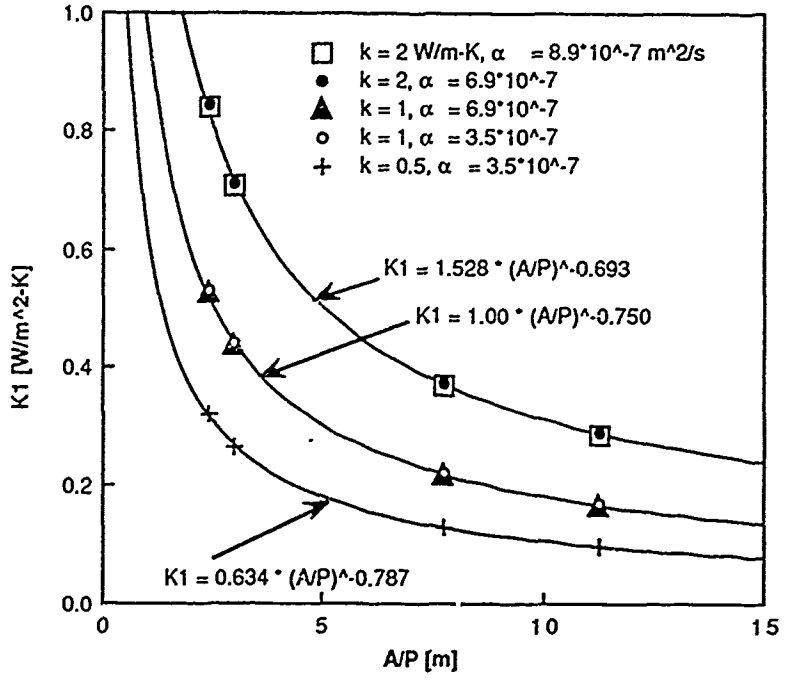

(a)

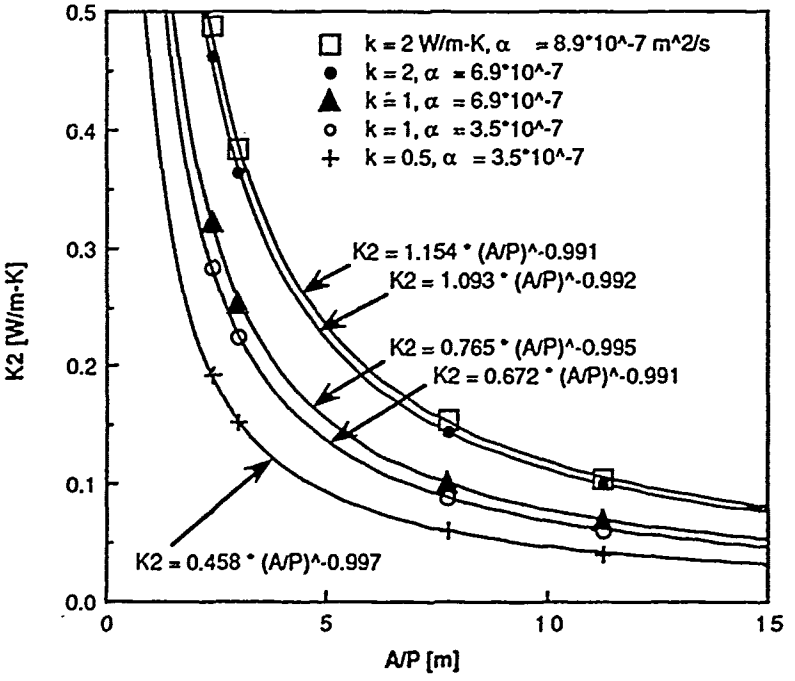

(b)

Figure 8. Influence of soil properties on area dependence of floor heat loss: (a) mean and (b) amplitude.

Table 9

Thermal Conductivity Influence on Floor Center and Edge Heat Loss Values for Two Uninsulated Slabs in Philadelphia, PA, January 21

Property Set	k (W/m-K)	q_{center} (W/m^2)	Δq_{center} (%)	$q_{edge,\,max}$ (W/m^2)	Δq_{edge} (%)	q_{avg} (W/m^2)	Δq_{avg} (%)
a) 12 x 12 m							
Base	1	1.8	0	69.0	0	7.9	0
A	2.0	3.5	94.4	78.9	14.4	12.2	54.4
C	0.5	0.9	-50.0	55.5	-19.6	4.7	-40.5
b) 45 x 45 m							
Base	1	0.7	0	68.9	0	2.7	0
A	2.0	1.4	100.0	78.8	14.4	4.5	66.7
C	0.5	0.4	-42.9	55.5	-19.5	1.6	-40.7

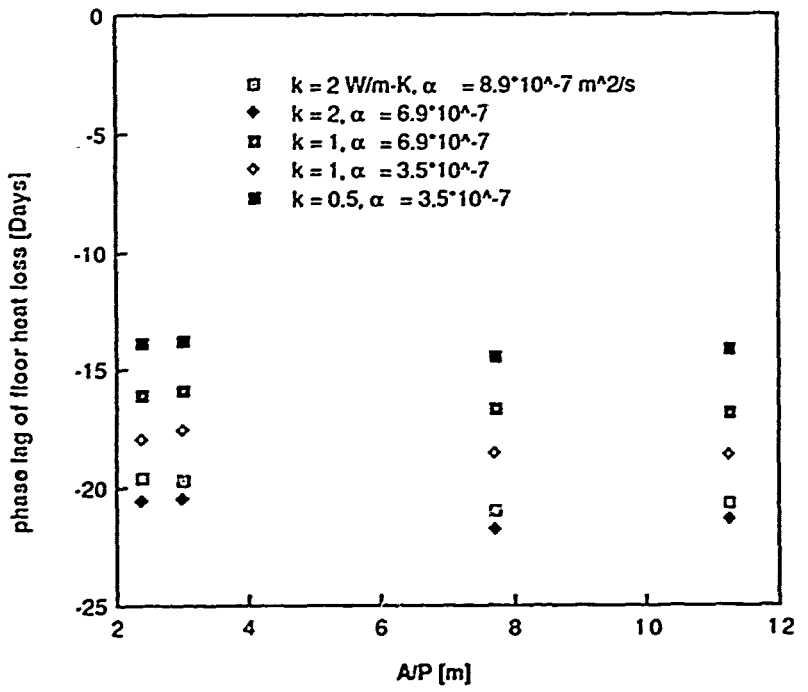

Figure 9. Effects of thermal conductivity and thermal diffusivity on phase lag of floor heat loss.

Effect of Insulation

A recent DOE report[41] documents the large potential for energy savings through the insulation of building foundations. Results of this study also indicate that (1) energy consumption due to heat flows through uninsulated foundations may contribute 20 percent or more of a building's energy budget and (2) perimeter insulation can reduce these energy losses by 50 percent or more.[42] Consequently, the effect of insulation on the proposed model is of great practical interest. An examination of insulation effects was included in this study to determine how well Eq 26 could accommodate insulated slab floors. Limitations on the range of parameters considered in the series I insulation runs included.

- Minneapolis weather only
- Insulation limited to 1 or 2 in. thicknesses of expanded extruded polystyrene board (k = 0.029 W/m-K)
- Two configurations: edge + 1 m under slab perimeter and edge + entire bottom surface of slab.

Although this set of parameters is far from comprehensive, these cases serve well to demonstrate the effects of insulation on floor heat loss as reflected in the coefficients of Eq 26.

The simplified model seems quite capable of handling insulated floors without structural changes. Insulation does, however, have a significant effect on the model coefficients. Coefficient values for the uninsulated slab and the two perimeter insulated cases appear in Table 10. As insulation is added, the area dependence of both the steady and periodic components of heat transfer increases. As in previous cases, the steady state component is affected more strongly. The maximum fractional change in d_1 is more than three times greater than the corresponding change in d_2. With 2 in. of insulation on the perimeter, d_2 still deviates from -1 by only 7.8 percent, thus, the strict perimeter dependence of the periodic heat loss component is not seriously violated.

Figures 10 and 11 show the effect of insulation on daily low floor temperature during January. In Figure 10, the uninsulated case, daily low temperature is more than 10°C below the daily average and approaches freezing on several days. The range of low temperatures is approximately 8 °C during this period. When 2 in. of perimeter insulation are added to this floor, the difference between the daily average and low temperatures is reduced by more than half and variation in the daily low is also much smaller. An interesting and superficially contradictory effect of insulation demonstrated by these figures and the coefficient data in Table 10 is that a more uniform floor temperature distribution enhances the shape dependence of heat loss. By decreasing heat loss at the floor perimeter, insulation raises the contribution of interior area to total heat loss. Thus, while the floor temperature distribution is "less three-dimensional," heat transfer is *more* three-dimensional. In light of this fact, the predictions of perimeter heat loss factor methods may be especially misleading for highly insulated floors, regardless of the configuration.

Figure 12 shows daily averaged heat loss from a 12 by 12 m floor for three different insulation treatments. The raw results have been smoothed to facilitate comparison. As insulation is added to the bare slab, both the mean and amplitude of the daily heat loss decrease. Consequently, the maximum heat loss is reduced by a much greater amount than the minimum. The resulting benefit in winter heating load avoided is much greater than the penalty paid in cooling lost during the summer. The result for full 1 in.-thick insulation, which is not shown, would lie almost directly on top of the

[41]K. Labs et al.
[42]W. P. Bahnfleth.

curve for the 2-in.-thick, 1-m wide configuration. The nearly identical performance of these two much different treatments illustrates the importance of effective insulation placement. The full 1-in.-thick treatment requires 64 percent more material to achieve the same performance as the heavy perimeter insulation configuration.

Table 10

Comparison of Daily Averaged Heat Loss Model Coefficients for Three Insulation Treatments in Minneapolis, MN

Insulation Treatment	c_1	d_1	c_2	d_2
Uninsulated	0.997	-0.735	0.759	-0.999
1" Thick, 1 m wide	0.603	-0.623	0.408	-0.953
2" Thick, 1 m wide	0.475	-0.570	0.308	-0.921

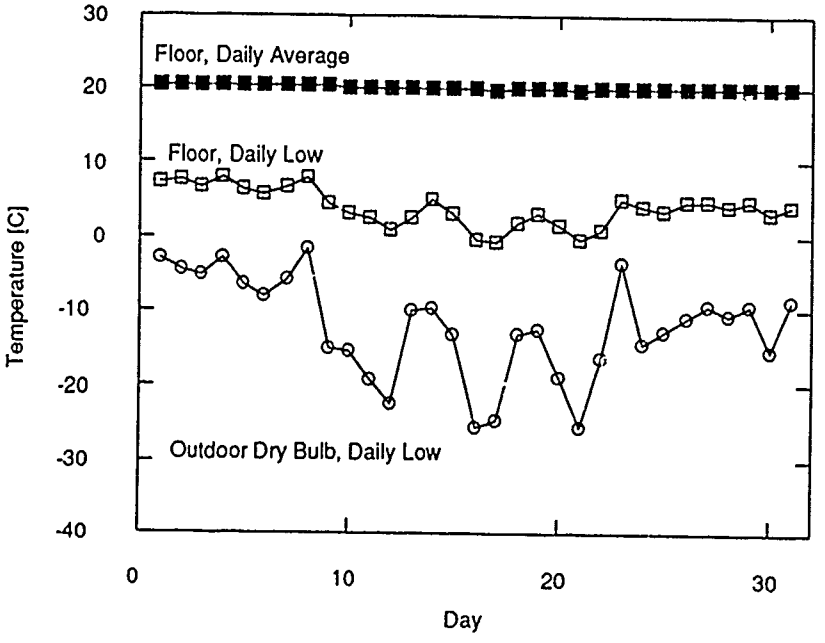

Figure 10. January daily low and average floor surface temperatures for a 12 by 12 m uninsulated floor in Minneapolis, MN.

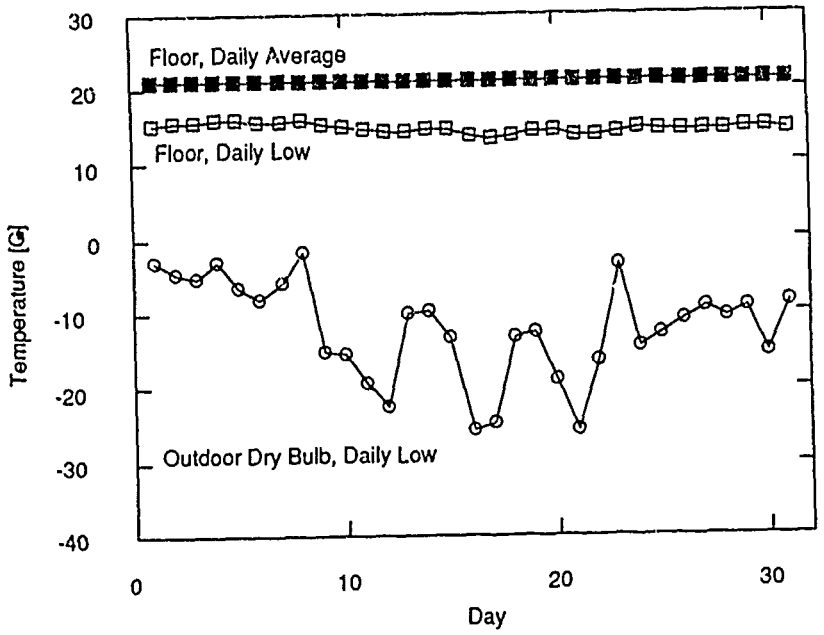

Figure 11. January daily low and average floor surface temperatures for a 12 by 12 m floor with 1 m of 2-in.-thick perimeter insulation in Minneapolis, MN.

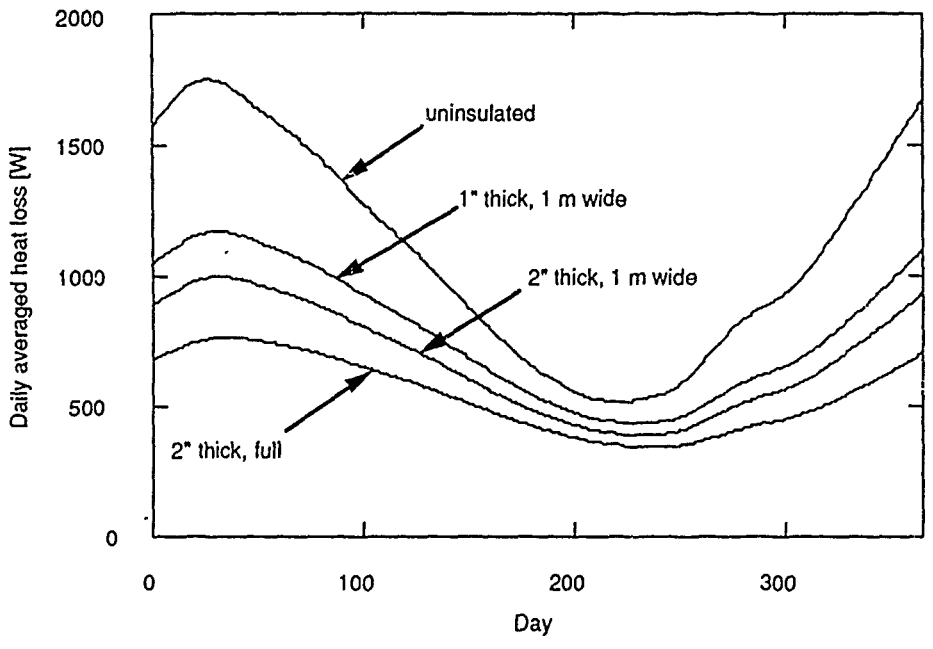

Figure 12. Smoothed, daily-averaged heat loss from a 12 by 12 m Minneapolis slab floor with various insulation treatments.

Summary

This chapter has presented a potentially useful approach for the manual estimation of heat loss from slab floors. The most significant features of this model are (1) separation of heat loss into mean and periodic components, (2) the scaling of geometric effects by the floor length scale, A/P, and (3) use of ground surface temperature as an ambient reference condition. It has been shown that this model gives a good approximation of results obtained from a detailed, three-dimensional numerical model under conditions of varying shape and size, for a range of soil properties, and when insulation is added to a floor to reduce its energy consumption. The model does not explicitly account for changes in soil properties or floor construction, but can be made to give accurate estimates through the use of multiple coefficient sets. This model also is useful as a tool for interpreting the effects of various parameters on floor heat transfer rates. The A/P scaling approach embodied in this model is of theoretical significance and may contribute to the development of other efficient techniques for earth-coupled heat transfer estimation.

4 TRANSFER FUNCTION ALGORITHM

This chapter outlines a technique for calculating the heat flux through a slab-on-grade floor using response factor methodology. The algorithm developed is compatible with existing detailed hourly energy as well as simpler analysis programs. Input for the method is dependent on the undisturbed ground temperatures calculated during the data base development described in Chapter 2. A portion of the heat flux data from Chapter 2 is used to evaluate the accuracy of this algorithm.

Overview

Detailed hourly energy analysis programs such as BLAST use response factor methodology to calculate building heat loss.[43] These response factors are developed from the one-dimensional solution of the Fourier equations for each building surface. This method has proven reliable for above-ground building components, but the technique used in applying it to ground-contact surfaces has oversimplified the ground heat transfer process. Unidimensional analysis assumes that heat loss (or gain) through earth-contact surfaces is a function of only two temperatures--generally the surface temperature and the deep-ground temperature. In fact, most earth-contact surfaces "see" at least two temperatures: the outdoor ground-surface temperature and the deep-ground temperature. This condition is recognized by manual slab-on-grade heat loss calculations, which make separate determination of edge loss and core loss. In addition, one-dimensional analysis assumes a linear temperature profile, which is not a realistic representation of the temperature profile beneath slab-on-grade surfaces. Response factor methodology could be better applied to earth-contact surfaces if the multidimensionality of the problem is acknowledged and a procedure developed to calculate multidimensional heat transfer coefficients for the ground.

Ceylan and Myers[44] developed a response-coefficient method for multidimensional heat conduction problems which is substantially more efficient than finite-difference or finite-element methods. Seem[45] devised a procedure for calculating multidimensional transfer functions that eliminates some of the computationally expensive steps of the Ceylan and Myers method. These multidimensional methods have been applied to strictly geometrical heat conduction problems. This study extends these techniques to the more conceptual environment of simplified models. Specifically, these concepts are applied to the problem of heat flux through slab-on-grade surfaces.

Concept

Many physical systems, including thermodynamic systems, can be approximated using lumped-system analysis. In this approach, the system is described as a series of lumped, linear, dynamic elements defined by ordinary differential equations. The network analogy provides a simple visualization of this concept. In a network model of a thermal system, temperatures are represented by nodes with a linear temperature distribution between each pair of nodes. Physical properties are considered to be uniform between each pair of nodes, but can vary among pairs. Energy balance equations are written for each node and the system of equations is solved for unknown temperatures

---

[43] D. C. Hittle, *Calculating Building Heating and Cooling Loads Using the Frequency Response of Multilayered Slabs*, Technical Manuscript E-169/ADA097597 (USACERL, February 1981).

[44] H. T. Ceylan and G. E. Myers, "Long-Time Solutions to Heat-Conduction Transients With Time-Dependent Inputs," *ASME Journal of Heat Transfer*, Vol 102 (February 1980).

[45] J. E. Seem, *Modeling of Heat Transfer in Buildings*, Ph.D. Thesis (University of Wisconsin, 1987).

and heat fluxes. The validity of the system model depends on the accuracy of the assumptions of uniform temperature at each node and linearity between nodes.

The matrices forming the energy balance equations of the nodes can be constructed using state space representation, resulting in the state equation:

$$\frac{\partial X}{\partial t} = \mathcal{A}X + \mathcal{B}U \qquad \text{[Eq 27]}$$

and the output equation:

$$Q = \mathcal{C}X + \mathcal{D}U \qquad \text{[Eq 28]}$$

The matrix **X** contains the unknown temperatures (state variables). **U** is the matrix of known temperatures (input variables). **Q** is the matrix of fluxes (output variables). *A*, *B*, *C*, and *D* are coefficient matrices. The size of the matrices and the values of the elements will be determined by the specific model. Once the coefficient matrices are defined and the input values identified, the first-order differential equations can be solved. Seem's method[46] is used to solve the system of equations. In this formulation, the time series of input variables is modeled as a continuous piecewise linear function by:

$$U(\tau) = U_t + \frac{(\tau - t)}{\delta}(U_{\tau - \delta} - U_t) \qquad \text{[Eq 29]}$$

Using this function for the inputs, the differential equations are solved and substituted for **X** in Eq 28, resulting in an equation that relates system outputs to inputs. This equation is known as the "transfer function equation" and is of the form:

$$Q_t = \sum_{j=0}^{n} (S_j U_{t-j\delta}) - \sum_{j=0}^{n} (c_j Q_{t-j\delta}) \qquad \text{[Eq 30]}$$

where:

- Qi = vector of output variables (heat flux) at time i
- Sj = transfer function matrix for temperature inputs at time j
- j = designator identifying a point in time, where j = 0 is the current time
- j = 1 is one time step before the current time and so on
- t = time of interest
- δ = time step
- U_i = vector of input variables (known temperatures) at time i
- c = scalar constant for adjusting the effect of previous outputs on the output at the time of interest.

A transfer function is defined as the ratio of the output variables of a system in state space to its input variables (also in state space). In this way, the transfer function represents the dynamics of a linear time-invariant system. The transfer function matrices depend on the system and inputs, but only

---

[46]J. E. Seem.

on the functional form of the inputs; therefore, any input that can be modeled adequately by the continuous piecewise linear function noted above can be used with the transfer function matrices to model its effect on the system. This option is particularly useful in modeling building systems where the input conditions of climate vary greatly in time and geographic location.

Model Development

The system modeled for this study is a square slab-on-grade. The model proposed is a seven-node network with three state variables and four inputs (Figure 13). The known temperatures (or inputs) are the daily average slab core region temperature (T_b), the daily average slab edge region temperature (T_e), the daily average ground surface temperature (T_f), and the deep-ground temperature (T_d). The three state variables, the temperatures at the remaining nodes (T_1, T_2, and T_3), are allowed to float and consequently have some thermal capacitance attributed to them. The temperature nodes are related to each other as shown in the figure. Between attached pairs of temperature nodes, there is some thermal resistance. These resistances and capacitances are defined below and in Amber.[47]

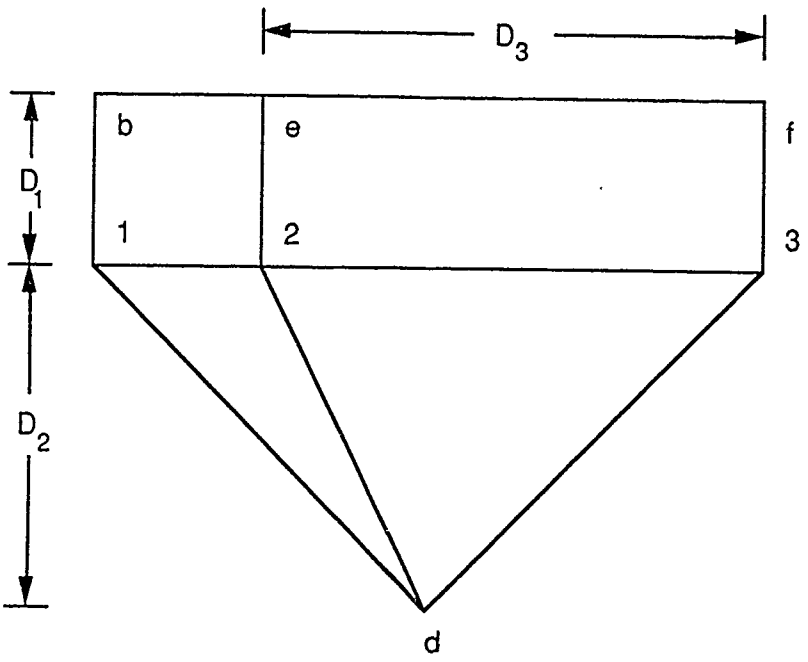

Figure 13. Seven-node network model.

[47] J. A. Amber, *Multiple-Input Transfer Function Model of Heat Transfer From Square Slab Floors*, M.S. Thesis (University of Illinois, May 1989); also published as USACERL Technical Manuscript E-89/14/ ADA219193 (November 1989).

Basic Equations

Energy balance equations are written for each node, resulting in four state equations of the form:

$$C_i \frac{\partial T_i}{\partial t} = \sum_{j=1}^{7} G_{ij} (T_j - T_i) \qquad \text{[Eq 31]}$$

for i = 1 to 4, and three state output equations of the form:

$$Q_i = \sum_{j=1}^{7} G_{ij} (T_j - T_i) \qquad \text{[Eq 32]}$$

for i = 1 to 3, where:

C_i = thermal capacitance at node T_i

$G_{ji}=\frac{1}{R_{ji}}$ = inverse of the thermal resistance between nodes T_j and T_i,

These seven equations can be written more conveniently in matrix form:

$$\frac{\partial X}{\partial t} = \mathcal{A}X + \mathcal{B}U \qquad \text{[Eq 33]}$$

and:

$$Q = \mathcal{C}X + \mathcal{D}U \qquad \text{[Eq 34]}$$

where:

$$\frac{\partial X}{\partial t} = \begin{pmatrix} \frac{\partial T_1}{\partial t} \\ \frac{\partial T_2}{\partial t} \\ \frac{\partial T_3}{\partial t} \end{pmatrix} \qquad \text{[Eq 35]}$$

$$X = \begin{pmatrix} T_1 \\ T_2 \\ T_3 \end{pmatrix} \qquad \text{[Eq 36]}$$

$$U = \begin{pmatrix} T_b \\ T_f \\ T_d \\ T_e \end{pmatrix}$$

[Eq 37]

$$Q = \begin{pmatrix} Q_b \\ Q_f \\ Q_d \\ Q_e \end{pmatrix}$$

[Eq 38]

$$\mathcal{A} = \begin{pmatrix} \frac{-G_{1b} - G - G_{1d}}{C_1} & \frac{G_{12}}{C_1} & 0 \\ \frac{G_{12}}{C_2} & \frac{-G_{2e} - G_{12} - G_{23} - G_{2d}}{C_2} & \frac{G_{23}}{C_2} \\ 0 & \frac{G_{23}}{C_3} & \frac{-G_{3f} - G_{23} - G_{3d}}{C_3} \end{pmatrix}$$

[Eq 39]

$$\mathcal{B} = \begin{pmatrix} \frac{G_{1b}}{C_1} & 0 & \frac{G_{1d}}{C_1} & 0 \\ 0 & 0 & \frac{G_{2d}}{C_2} & \frac{G_{2e}}{C_2} \\ 0 & \frac{G_{3f}}{C_3} & \frac{G_{3d}}{C_3} & 0 \end{pmatrix}$$

[Eq 40]

$$\mathcal{C} = \begin{pmatrix} G_{1b} & 0 & 0 \\ 0 & 0 & G_{3f} \\ G_{1d} & G_{2d} & G_{3d} \\ 0 & G_{2e} & 0 \end{pmatrix}$$

[Eq 41]

$$D = \begin{pmatrix} -G_{1b}-G_{bc} & 0 & 0 & G_{bc} \\ 0 & -G_{3f}-G_{cf} & 0 & G_{cf} \\ 0 & 0 & -G_{1d}-G_{2d}-G_{3d} & 0 \\ G_{bc} & G_{cf} & 0 & -G_{bc}-G_{cf}-G_{2c} \end{pmatrix} \quad \text{[Eq 42]}$$

The coefficient matrices **A, B, C,** and **D** define the relationships of all temperature regions in the system to all others. They involve geometric factors such as the area through which heat is transferred from one region to another, and physical properties such as the density and thermal conductivity of various regions. The goal of defining the elements of the coefficient matrices is to make it possible to generate transfer function equations for any system from its basic physical parameters rather than as is frequently done in electromechanical systems--by testing the system itself. Because the important aspect of the equations is the thermal relationships between regions, the model is not strictly geometrical. The first step in defining the matrix coefficients is identifying the properties that comprise the elements of G and C. The basic form allows for the description of several heat transfer mechanisms, given the appropriate temperatures. For conduction, the equation becomes:

$$Q = kA\frac{\partial T}{\partial x} \quad \text{[Eq 43]}$$

or, in the spatially discretized form used for this model:

$$Q_{ij} = \left(\frac{k_{ij}A_{ij}}{L_{ij}}\right)(T_i - T_j) \quad \text{[Eq 44]}$$

In this case G_{ij} is defined as the conductance,

$$G_{ij} = \frac{kA}{L} \quad \text{[Eq 45]}$$

where:

k_{ij} = thermal conductivity applicable to the volume between nodes i and j
A_{ij} = cross-sectional area through which heat is transferred between nodes i and j
L_{ij} = distance between nodes i and j.

The thermal capacitance C is derived from the transient equation:

$$Q = \rho c_p V\frac{\partial T}{\partial t} \quad \text{[Eq 46]}$$

so that:

$$C_i = \rho_i c_{p_i} V_i \qquad \text{[Eq 47]}$$

where:

ρ_i = density of the region of soil at T_i
c_{pi} = specific heat of the region of soil at T_i
V_i = volume of the region of soil at T_i.

Both thermal conductance, G_{ij}, and thermal capacitance, C_i, are composed of geometrical factors (L_{ij}, A_{ij}, V_i) as well as soil properties (k_{ij}, ρ_i, and c_{pi}). These factors will be discussed separately.

Geometry

Bahnfleth's study[48] of undisturbed ground temperature patterns shows two distinctly different zones of temperature fluctuation: (1) a relatively fast zone near the ground surface where the temperature changes are in scale with the temperature changes of the forcing temperature and (2) a slower zone where temperature fluctuations are strongly damped. Because the response rate of the near-surface zone is more similar to the response rate of typical building components than to that of the rest of the earth, it was decided to model the near-surface earth and the rest of the earth as attached but distinct components. The point of separation for these zones is the diurnal penetration depth, or roughly 0.5 m below the surface. The temperature at this point remains nearly constant over each day at that day's daily average ground surface temperature.

Horizontal maps of ground temperature beneath buildings show a circular pattern: thus, a cylindrical coordinate system was used to produce an axisymmetric two-dimensional model. Horizontal temperature nodes are set at the slab center, the edge-equivalent radius, and the location where the ground temperature is unaffected by the building (far-field). The edge-equivalent radius is calculated as the radius of a circle of equivalent slab perimeter, or:

$$r_p = \frac{P}{2\pi} \qquad \text{[Eq 48]}$$

Vertical temperature nodes are set at the diurnal penetration depth of the surface temperature wave (about 0.5 m below the surface), the annual penetration depth (about 15 m below the surface), and the depth of the point of inflection or knee of the undisturbed temperature profile (about 4 m below the surface). Studies of underground temperature patterns[49] show a shape that could be approximated by linear temperature profiles between these temperature nodes (Figure 14). The area-equivalent radius is used for calculations in the vertical plane. It is calculated as the radius of the circle that has the same area as the slab, i.e.:

$$r_a = \sqrt{\frac{A}{\pi}} \qquad \text{[Eq 49]}$$

---

[48] W. P. Bahnfleth.

[49] W. P. Bahnfleth; P. H. Shipp; T. Kusuda and J. W. Bean, "Simplified Methods for Determining Seasonal Heat Loss From Uninsulated Slab-on-Grade Floors," *ASHRAE Transactions*, Vol 90 (1984).

Although this model cannot be reproduced graphically, it accounts for both the perimeter and area effects of ground-coupled heat transfer.

Geometrical factors appear in three matrices--A, L, and V. A and V are both symmetric 7 X 7 matrices. For the seven-node network model, not all of the nodes are connected. Elements that relate unconnected nodes to each other become 0, so that:

$$A = \begin{pmatrix} 0 & A_{12} & 0 & A_{1b} & 0 & A_{1d} & 0 \\ A_{12} & 0 & A_{23} & 0 & 0 & A_{2d} & A_{2e} \\ 0 & A_{23} & 0 & 0 & A_{3f} & A_{3d} & 0 \\ A_{1b} & 0 & 0 & 0 & 0 & 0 & A_{be} \\ 0 & 0 & A_{3f} & 0 & 0 & 0 & A_{fe} \\ A_{1d} & A_{2d} & A_{3d} & 0 & 0 & 0 & 0 \\ 0 & A_{2e} & 0 & A_{be} & A_{fe} & 0 & 0 \end{pmatrix} \qquad \text{[Eq 50]}$$

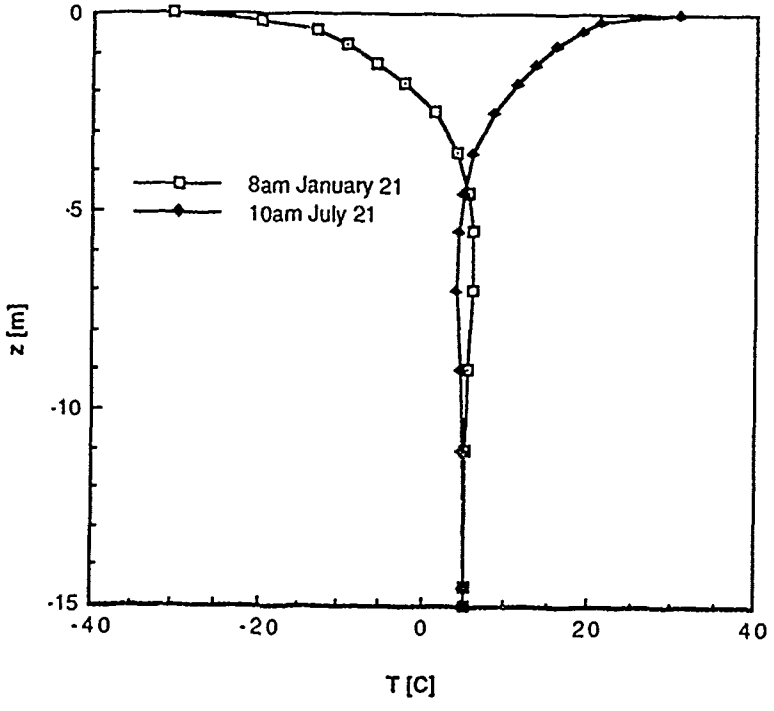

Figure 14. Undisturbed ground temperature profile.

and:

$$L=\begin{pmatrix} 0 & L_{12} & 0 & L_{1b} & 0 & L_{1d} & 0 \\ L_{12} & 0 & L_{23} & 0 & 0 & L_{2d} & L_{2e} \\ 0 & L_{23} & 0 & 0 & L_{3f} & L_{3d} & 0 \\ L_{1b} & 0 & 0 & 0 & 0 & 0 & L_{be} \\ 0 & 0 & L_{3f} & 0 & 0 & 0 & L_{fe} \\ L_{1d} & L_{2d} & L_{3d} & 0 & 0 & 0 & 0 \\ 0 & L_{2e} & 0 & L_{be} & L_{fe} & 0 & 0 \end{pmatrix} \qquad \text{[Eq 51]}$$

where the subscripts refer to the path; i.e., A_{ij} is the area through which heat is transferred from T_i to T_j.

V is the vector:

$$V=\begin{pmatrix} V_1 \\ V_2 \\ V_3 \end{pmatrix} \qquad \text{[Eq 52]}$$

The definition of the elements, or network parameters, A_{ij}, L_{ij}, V_i is, in part, independent of the model structure, but is based on the geometry presented above and is described further under Network Parameter Specification below and in Amber.[50]

Soil Properties

Soil properties are represented by another 7 X 7 symmetric matrix:

$$k=\begin{pmatrix} 0 & k_{12} & 0 & k_{1b} & 0 & k_{1d} & 0 \\ k_{12} & 0 & k_{23} & 0 & 0 & k_{2d} & k_{2e} \\ 0 & k_{23} & 0 & 0 & k_{3f} & k_{3d} & 0 \\ k_{1b} & 0 & 0 & 0 & 0 & 0 & k_{be} \\ 0 & 0 & k_{3f} & 0 & 0 & 0 & k_{fe} \\ k_{1d} & k_{2d} & k_{3d} & 0 & 0 & 0 & 0 \\ 0 & k_{2e} & 0 & k_{be} & k_{fe} & 0 & 0 \end{pmatrix} \qquad \text{[Eq 53]}$$

[50]J. A. Amber.

and two vectors:

$$\rho = (\rho_1 \ \rho_2 \ \rho_3) \qquad \text{[Eq 54]}$$

and:

$$c_p = (c_{p_1} \ c_{p_2} \ c_{p_3}) \qquad \text{[Eq 55]}$$

Thermal properties of the soil can be defined separately for each energy balance equation. Individually, the energy balance equations assume constant thermal properties. Consequently, the properties are defined as the "effective" value of the thermal properties in the region specified by the equation. The need for an "effective" conductivity in discrete models is described more thoroughly by Bahnfleth[51] and Patankar.[52] Effective conductivity is defined as:

$$k_e = \frac{\Sigma l_k}{\Sigma \frac{l_k}{k_k}} \qquad \text{[Eq 56]}$$

where:

l_k = the thickness of layer k
k_k = the conductivity of layer k.

Calculated from this equation, k_{ij} is the effective value of the soil conductivity in the region through which heat transfers between T_i and T_j.

The units of k are specified during programming as J/day-m-K. This step is necessary because of the small size of components of the calculated transfer function coefficient matrices. Without this adjustment, many of the components approached zero, causing the calculations to fail. After the flux was calculated, the units were converted back to W/m-K before reporting.

Inputs

The inputs to the transfer function equation are (referring to Figure 13) the temperatures of the slab core area (T_b) and the slab edge area (T_e), and the undisturbed ground temperatures near the surface (T_f) and in the deep ground (T_d). Because the "top" nodes are defined at the diurnal penetration depth, their temperatures can be approximated by the daily average of the surface temperature, i.e., T_b = the daily average slab center temperature and T_f = the daily average ground surface temperature. The undisturbed ground-surface and deep-ground temperatures can be determined *a priori* using one of a variety of algorithms.

---

[51]W. P. Bahnfleth.
[52]S. V. Patankar.

Network Parameter Specification

The network parameters are the elements that compose the geometrical matrices A, L, and V. Their definition depends on the method of discretizing the system geometry. In other words, the magnitude of the element depends on the sizes of the regions assumed to be at the specified temperatures. Because few of the regions are actually isothermal, the allocation of area and volume to a specific temperature must be based on some method or algorithm. In this study, the heat transfer areas are postulated from basic knowledge of the typical temperature profiles in and around slab-on-grade surfaces. The postulates are tested and modified empirically to tailor them to the model. Details of this procedure are given elsewhere.[53]

Once the model is established, a test system is defined to describe a specific set of building and environmental input conditions. These data are input to the programmed model and the results are compared with data from the data base described in Chapter 2. The data set used for evaluation of the transfer function model is series E presented in the Appendix. This set contains data for four climates and four different building size/shape configurations for the most severe climate, Minneapolis, MN.

Description of Test System

Geometry. The test system is based on the initial assumption of a square slab. Data were available from series E for two sizes of square slabs, a 12 by 12 m square and a 45 by 45 m square. Figure 15 shows the series E flux per unit area data for these two slabs for a calendar year in Minneapolis (the most severe of the four location sets in series E). Due to the dominance of the edge effect, the annual flux variation is much greater for the smaller slab. If the effect of the balance between the perimeter and edge losses is to be accommodated, it is important that the test system exhibit this effect strongly. Therefore, the smaller 12 by 12 m slab was used as the primary test system.

Soil Properties. Although the system model can support variable soil properties, this capability was not tested in this study. Series E heat flux data were calculated using constant soil properties. The same properties were used in the test system.

Inputs. Data from Bahnfleth's one-dimensional semi-infinite solid model of the heat transfer in undisturbed earth were used as input for far-field and deep-ground nodes. Because the far-field node was placed at the diurnal penetration depth, the daily average ground-surface temperature, rather than the hourly ground-surface temperature, was used as input to the multiple input transfer function model. The deep-ground temperature was defined as the annual average of the ground-surface temperatures calculated by the semi-infinite solid model.

Exact data for the daily average slab center and slab edge temperatures were not available from the series E data. This lack of data is typical of hourly energy analysis programs that assume isothermal surfaces. Therefore, although it is possible in the network mode to include a temperature difference between the slab center and the slab edge, daily average slab surface temperatures (which are equal to the ground temperature at the diurnal penetration depth) were used for both of these temperatures. The network parameters developed under the assumption of an isothermal slab should be appropriate for application to energy analysis programs, such as 3LAST, that use the same assumption.

---

[53] J. A. Amber.

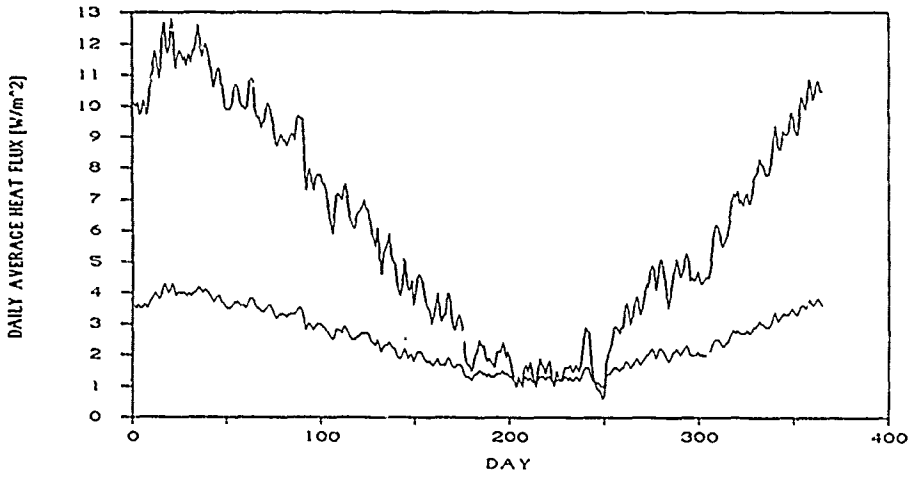

Figure 15. Finite difference model of two square slabs.

Series E included data for four locations, as described earlier (Minneapolis, Medford, Philadelphia, and Phoenix). To develop the most responsive model network parameters, the most rigorous weather conditions were used. Inspection of the daily average air temperature plots for the four locations indicated that the weather data for Minneapolis would provide the most demanding conditions for the model. In addition to a large annual temperature variation, the temperature variation from day to day is also greater in the Minneapolis data compared with the other three locations. During development of the network parameters, therefore, the data derived using Minneapolis weather were used to evaluate the accuracy of the model fit. The model was then tested later at the remaining three locations.

Definition of Network Parameters.

The geometrical definition of network parameters is based on a series of assumptions about the size and shape of the temperature regions beneath the slab as well as the geometry of the slab itself. The elements L_{ij} of the matrix L can be assigned simply as the distance between nodes i and j. Determination of the elements of A is more complex, however. Although the model is not strictly geometrical, the heat transfer areas can be initially postulated based on geometrical considerations and then refined by empirical methods.[54]

Program GTF[55] calculated the Ground Transfer Functions (GTFs) and scalar constants. Program QCALC[56] used the GTFs and the input temperatures with the transfer function equation to calculate the daily average heat flux. The results were divided by the slab area in order to have units compatible with those in series E data.

Final Definition and Testing

Final Definition

The final series of equations used to calculate the GTFs and scalar constants are given here in their final forms:

---

[54]J. A. Amber.
[55]J. A. Amber.
[56]J. A. Amber.

$$D_1 = 4.0\text{m} - 0.5\text{m} = 3.5\text{m}$$

[Eq 57]

$$D_2 = 15\text{m} - 4\text{m} = 11\text{m}$$

[Eq 58]

$$D_3 = 12.5\text{m}$$

[Eq 59]

$$d_1 = 1.0\text{m}$$

[Eq 60]

$$d_2 = 2.5 + 0.15(\text{characteristic length})$$

[Eq 61]

$$h_1 = \frac{D_1 + D_2}{2} = 7.25\text{m}$$

[Eq 62]

$$h_2 = 1.0\text{m}$$

[Eq 63]

$$h_3 = 0.1\text{m}$$

[Eq 64]

$$L_{1b} = L_{2e} = L_{3f} = D_1$$

[Eq 65]

$$L_{1d} = L_{2d} = L_{3d} = D_2$$

[Eq 66]

$$L_{fe} = L_{23} = D_3$$

[Eq 67]

$$r_p = \frac{P}{2\pi}$$

[Eq 68]

$$r_a = \sqrt{\frac{A}{\pi}} \qquad \text{[Eq 69]}$$

$$A_{be} = \frac{2\pi D_1 d_1}{\ln\left(\frac{r_p}{r_p - d_1}\right)} \qquad \text{[Eq 70]}$$

$$A_{ef} = \frac{2\pi D_1 D_3}{\ln\left(\frac{r_p + D_3}{r_p}\right)} \qquad \text{[Eq 71]}$$

$$A_{12} = \frac{2\pi D_2 d_1}{\ln\left(\frac{r_p}{r_p - d_1}\right)} \qquad \text{[Eq 72]}$$

$$A_{23} = 2\pi L_{23}\,(4.5)(\text{characteristic length}) \qquad \text{[Eq 73]}$$

$$A_{1b} = A_{1d} = \pi (r_a - d_1)^2 \qquad \text{[Eq 74]}$$

$$A_{3f} = A_{3d} = \pi (r_a + D_3)^2 - A_{1b} \qquad \text{[Eq 75]}$$

$$A_{2e} = A_{2d} = \pi (r_a + D_3)^2 - A_{1b} - A_{2e} \qquad \text{[Eq 76]}$$

$$V_1 = A_{1b} h_1 \qquad \text{[Eq 77]}$$

$$V_2 = A_{2e} h_2 \qquad \text{[Eq 78]}$$

$$V_3 = A_{3f} h_3 \qquad \text{[Eq 79]}$$

These equations were used to construct the geometry matrices **A, L,** and **V** (see Eqs 50 through 52) which, along with the soil property matrices k, ρ, and c_p (Eqs 53 through 55) were used to calculate the conductance and thermal capacitance matrices **G** and **C** (Eqs 45 and 47). These matrices, in turn, were are used to generate the coefficient matrices ***A, B, C***, and ***D***] (Eqs 39 through 42) which were used with Seem's method to calculate the final multiple input GTFs and scalar constants.

Validation

The final set of GTF coefficients and scalar constants calculated using the above equations were used to test the model for a variety of conditions, including diverse climates, slab size and shape, and sensitivity to input data.

Size. The effect of slab size on the model's accuracy is shown in Table 11. The model is quite accurate for relatively small (144 m^2) to relatively large (2025 m^2) square slabs, giving an error in total annual energy consumption of less than 3 percent (compared with the Finite Difference Model [FDM]) in both cases. The model is slightly more accurate overall for the larger slab based on the percentage of data within 15 percent of the FDM: 97 percent for the larger slab vs. 89 percent for the smaller slab.

Climate. The final GTF coefficients and scalar constants were used with environmental data for the remaining climates (Medford, Philadelphia, and Phoenix). Plots of the flux and differences for all four locations are given in Figures 16 through 19. Table 12 lists numerical data regarding the accuracy of the models.

For Minneapolis, Medford, and Philadelphia, the difference between the GTF model and the FDM is very nearly zero. In all cases, the difference is less than 1 W/m^2 except for a few days at the beginning of the annual cycle. In Phoenix, where the annual mean flux is approximately 1.5 W/m^2, an error of less than 1 W/m^2 can create a significant percentage error even when the actual value of the error is quite small.

Shape. This model was developed assuming a square slab and uses the circular soil isotherms evolving as the result of that geometry. Although it was not expected that this model would adequately model nonsquare slabs, the extent of the inaccuracy was unknown. Therefore, parameter sets were constructed based on the slab perimeters and areas and using the above equations. These parameter sets were used to calculate GTF coefficient matrices and scalar constants, and from them, daily average heat fluxes. The results are shown in Figures 20 and 21. Table 13 provides a numerical comparison of these results to the FDM results for the nonsquare slabs.

As anticipated, the model did not give good results for nonsquare slabs. The form of the errors indicated an inaccuracy in calculating the edge effect. In the summer when the area effect dominates, the difference between the FDM and the GTF model is nearly zero. However, as the ground-surface temperature drops and the edge effect becomes more important, the difference between the FDM and the GTF model shows an increasing underprediction of the slab heat loss.

Table 11

Results of the GTF Model for Slabs of Different Sizes*

Model	Area (m^2)	Mean Flux (W/M^2)	% of Data Within 15% of FDM (%)	Total Annual Energy Consumption (kWhr)	% Error in Total Energy Consumption (%)	Total Annual Difference in Energy Consumption (kWhr)
FDM	144	6.13	---	7716.9	---	---
GTF	144	6.19	89	7786.6	+0.9	+69.1
FDM	2025	2.50	---	44167.7	---	---
GTF	2025	2.42	97	42872.2	-2.9	-1295.5

*FDM = Finite Difference Model; GTF = Ground Transfer Function.

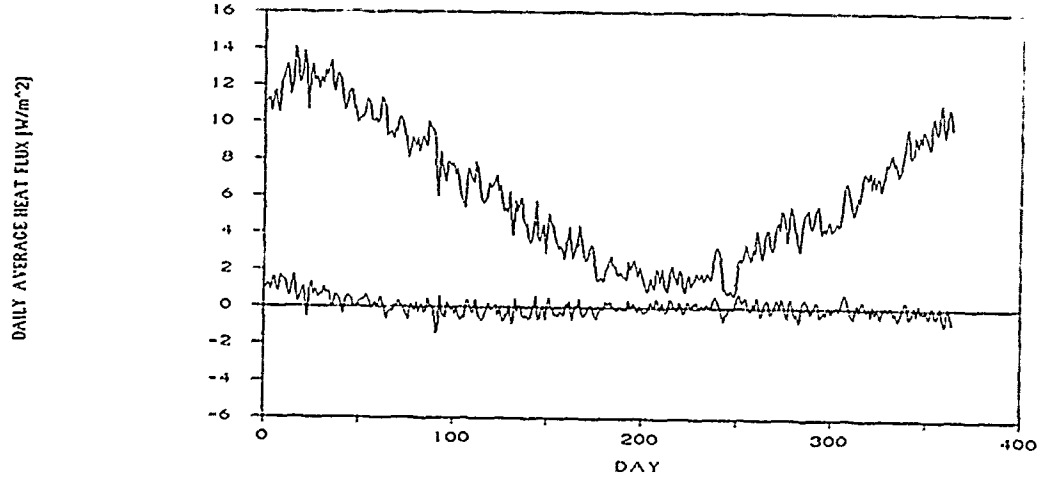

Figure 16. Heat flux--Minneapolis, MN.

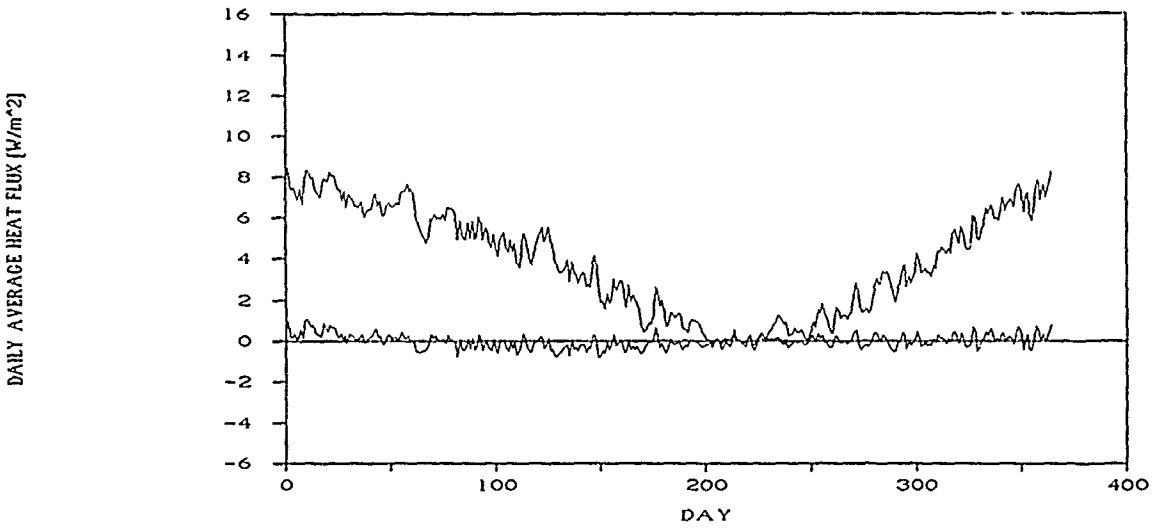

Figure 17. Heat flux--Medford, OR.

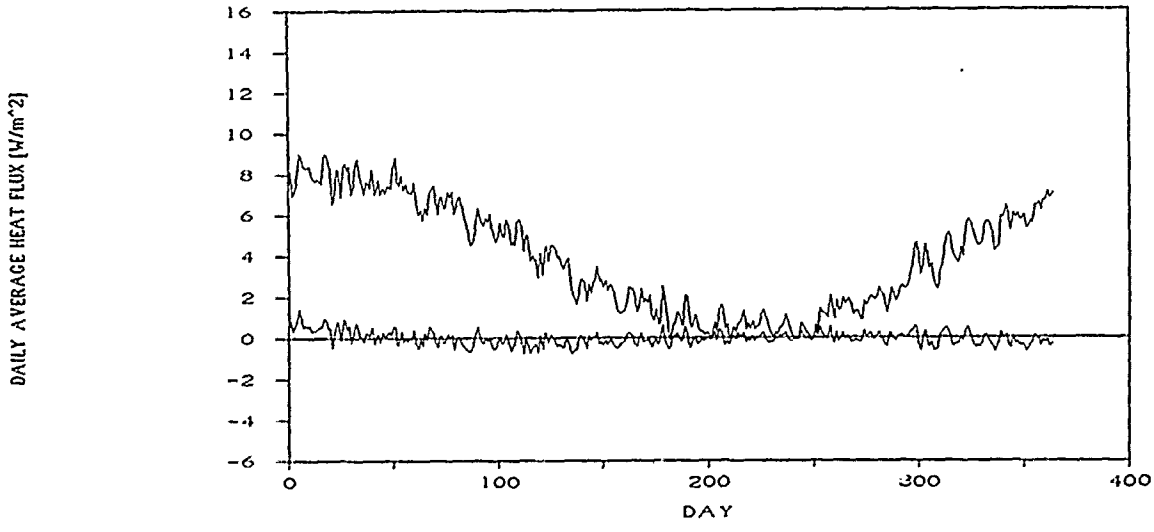

Figure 18. Heat flux--Philadelphia, PA.

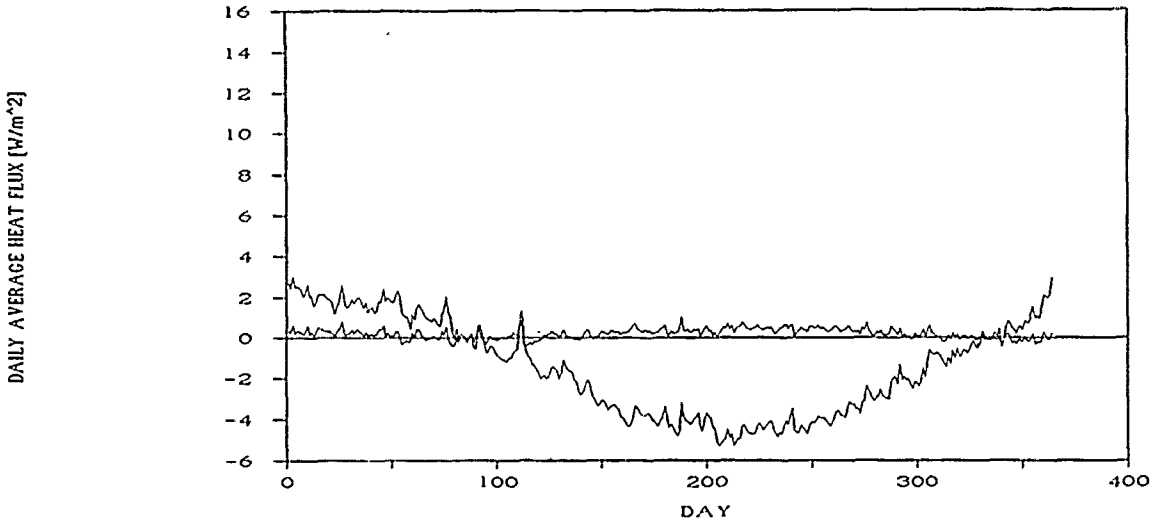

Figure 19. Heat flux--Phoenix, AZ.

Table 12

Results of the GTF Model for Various Locations*

Model	City	Mean Flux (W/M^2)	% of Data Within 15% of FDM (%)	Total Annual Energy Consumption (kWhr)	% Error in Total Energy Consumption (%)	Total Annual Difference in Energy Consumption (kWhr)
FDM	Minn	6.10	---	7716.9	---	---
GTF	Minn	6.19	89	7786.6	+0.9	+69.7
FDM	Med	3.87	---	4867.1	---	---
GTF	Med	3.86	78	4856.6	-0.2	-10.5
FDM	Phil	3.89	---	4893.7	---	---
GTF	Phil	3.87	78	4863.0	-0.6	-30.7
FDM	Phoe	-1.66	---	-2082.9	---	---
GTF	Phoe	-1.46	72	-1832.7	-12.0	+250.2

*FDM = Finite Difference Model; GTF = Ground Transfer Function.

Sensitivity to Inputs. It is important to understand the effect of the input data's accuracy on the results of the model, particularly if the required data are not available and must be approximated. Two plausible approximations are:

1. Substituting daily average outdoor dry-bulb temperature for daily average ground-surface temperature (T_f).

2. Substituting constant indoor air temperature for daily average floor-surface temperature (T_b) and daily average floor=edge temperature (T_e).

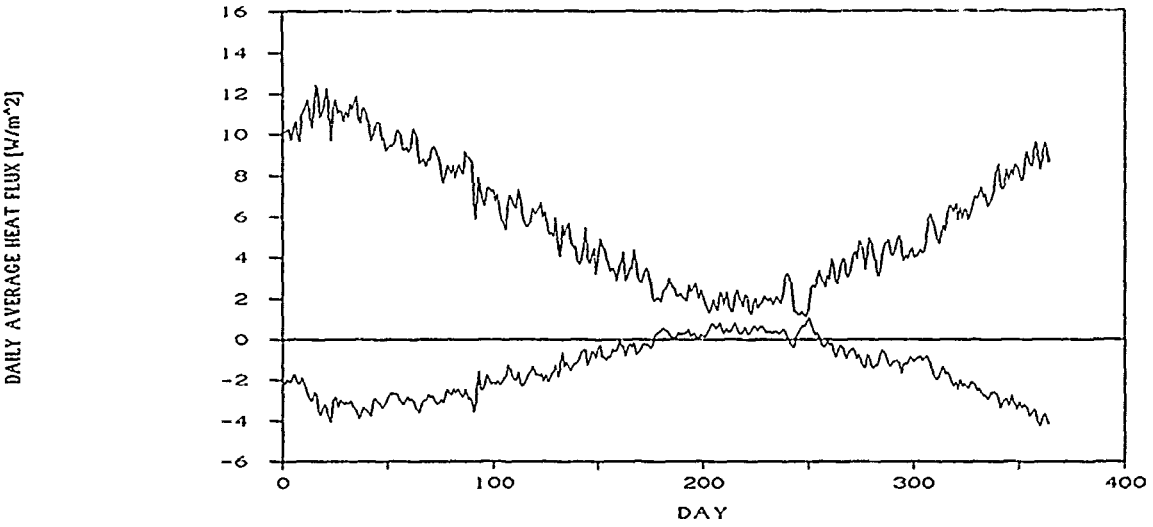

Figure 20. Heat flux--6 by 24 rectangle.

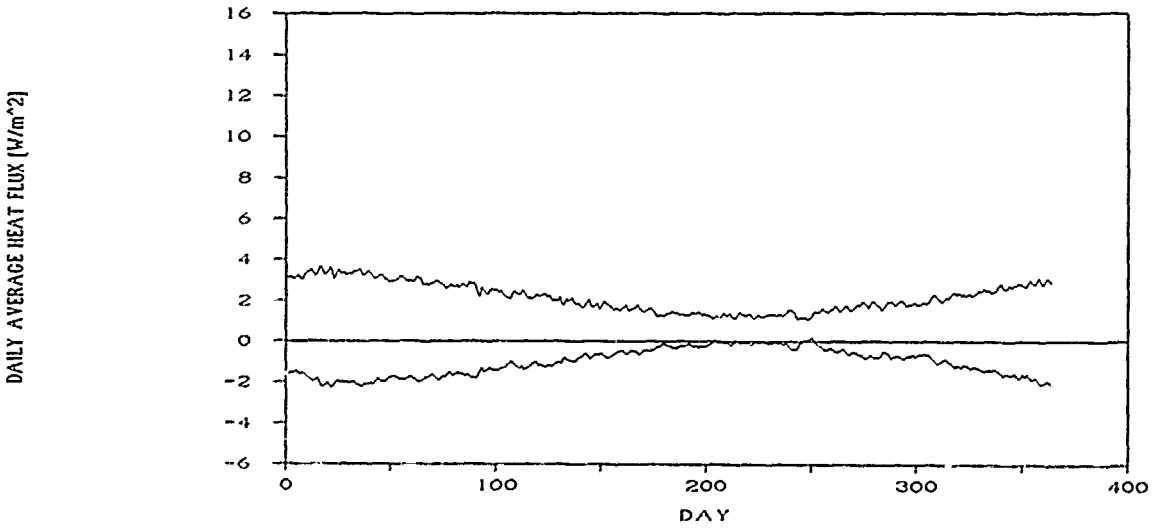

Figure 21. Heat flux--18 by 112 rectangle.

Table 13

Results of the GTF Model for Nonsquare Slabs*

Model	Slab Size (m^2)	Mean Flux (W/M^2)	% of Data Within 15% of FDM (%)	Total Annual Energy Consumption (kWhr)	% Error in Total Energy Consumption (%)	Total Annual Difference in Energy Consumption (kWhr)
FDM	6 x 24	7.30	---	9180.2	---	---
GTF	6 x 24	5.81	19	7305.2	-25.7	-1875.0
FDM	18 x 112	3.19	---	56405.2	---	---
GTF	18 x 112	2.18	19	38530.3	-31.7	-17874.9

*FDM = Finite Difference Model; GTF = Ground Transfer Function.

The input sensitivity tests used the GTF coefficients and scalar constants calculated from the final equations. When the approximation for one input data set was used, the remaining inputs were held identical to those in the original runs.

For the most part, the changes described in this section caused linear shifts of the flux curve. This linear shift appeared to be related mainly to the difference between the mean of the original data set and the mean of the substituted data. The slight changes in the shape of the input data curves did not have a great effect on the flux. It is probable, based on the linearity of the change, that altering more than one input would result in a linear shift related to the added effects of the individual changes.

Ground Surface Temperature Table 14 gives the numerical comparison of data resulting from substitution of the daily average outdoor air temperature for daily average ground-surface temperature as the input at T_f. The error in total energy consumption over the entire cycle ranges from 17.1 to 219.5 percent. Inspection of the graphical representation of the data (Figures 22 through 26) reveals a common pattern in the error. In all cases, the largest factor in the error is a positive linear offset which is greatest in Phoenix, where the temperature difference between air and ground temperatures is highest. The larger slab, where the edge effect is less substantial, changing far-field temperature has a much smaller effect on the results.

Slab Temperature. In this case, a constant value is substituted for the input data set. This substitution is convenient and practical in the many cases for which slab temperature is, in fact, nearly constant. Table 15 and Figures 27 through 31 give the results of this substitution. In assuming a constant temperature about 10 percent higher than the actual floor surface temperature, an error of roughly 10 percent is introduced. This error is primarily a linear shift, which appears typical of input data set changes. It seems to be mainly due to the difference between the mean value of the original data set and the mean of the substituted data. As in all other cases of input substitution, the effect is substantially smaller for the larger slab.

Network Parameters Based on Characteristic Length

Chapter 2 showed that heat flux through slabs of several different rectangular geometries can be calculated based on the slab characteristic length (A/P). This finding suggests that it may be possible to define the network parameters as functions of the soil geometry and slab characteristic length (A/P), thereby allowing the model to be used for nonsquare slabs.

As a crude test of this proposition, empirical models were developed for slabs of four different configurations: 12 by 12 m, 45 by 45 m, 6 by 24 m, and 18 by 112 m. Little attempt was made at this point to attach geometric significance to the network parameters: rather, each parameter set was adjusted based primarily on the quality of the resulting fit to each individual set of base case data. A parameter set was considered acceptable when more than 80 percent of the resulting data were within 15 percent of the corresponding FDM data and the error in total annual heat flux was less than 5 percent with the Minneapolis weather data. It should not be assumed that these parameter sets are in any way optimal. Once a set of parameters for each configuration was developed, the network parameters were compared to identify any patterns among the four cases.

Several relationships became evident. A_{3f}, A_{23}, V_1, and V_2 were of identical or similar value when the area of the slabs was (nearly) identical. This relationship is a strong indication that those parameters are functions of the slab area. Correspondingly, A_{bc}, and A_{2d} appeared to be functions of the slab perimeter. The remaining parameters were assumed to be functions of characteristic length, A/P.

Table 14

Results of Substituting Daily Average Outdoor Air Temperature for Daily Average Ground Surface Temperature*

Model	City	Edge Size (m^2)	Mean Flux (W/M^2)	% of Data Within 15% of FDM (%)	Total Annual Energy Consumption (kWhr)	% Error in Total Energy Consumption (%)	Total Annual Difference in Energy Consumption (kWhr)
FDM	Minn	12	6.13	---	7716.9	---	---
GTF	Minn	12	8.11	21	10197.4	+24.3	+2480.5
FDM	Med	12	3.87	---	4867.1	---	---
GTF	Med	12	4.55	49	5723.9	+17.6	+856.8
FDM	Phil	12	3.89	---	4893.7	---	---
GTF	Phil	12	5.65	12	7101.6	+45.1	+2207.9
FDM	Phoe	12	-1.66	---	-2082.9	---	---
GTF	Phoe	12	1.98	2	2488.8	-219.5	+4571.7
FDM	Minn	45	2.50	---	44167.7	---	---
GTF	Minn	45	2.92	47	51711.8	+17.1	+7544.1

*FDM = Finite Difference Model; GTF = Ground Transfer Function.

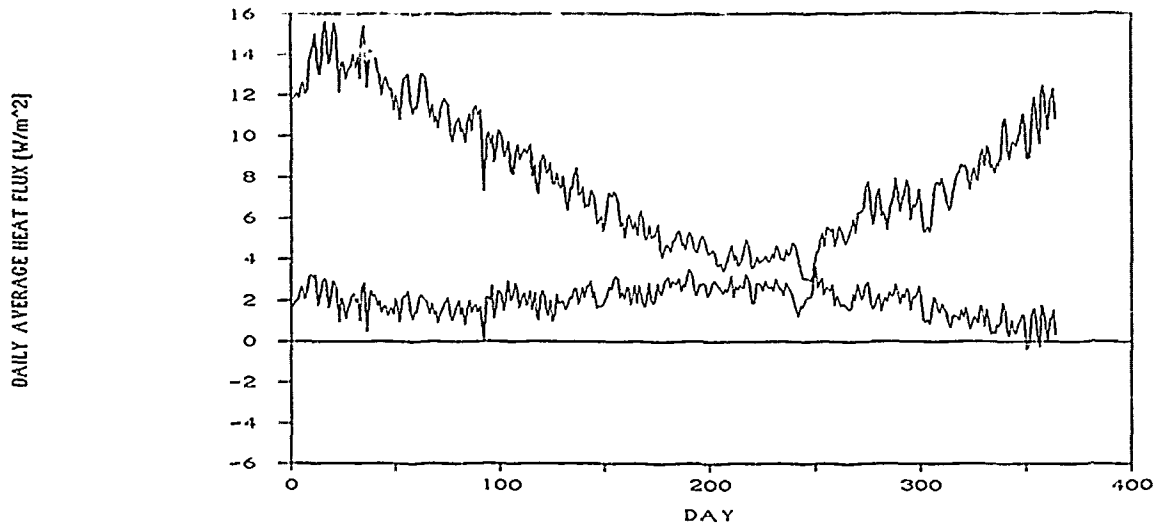

Figure 22. Heat flux--$T_f = T_{oa}$, Minneapolis, MN.

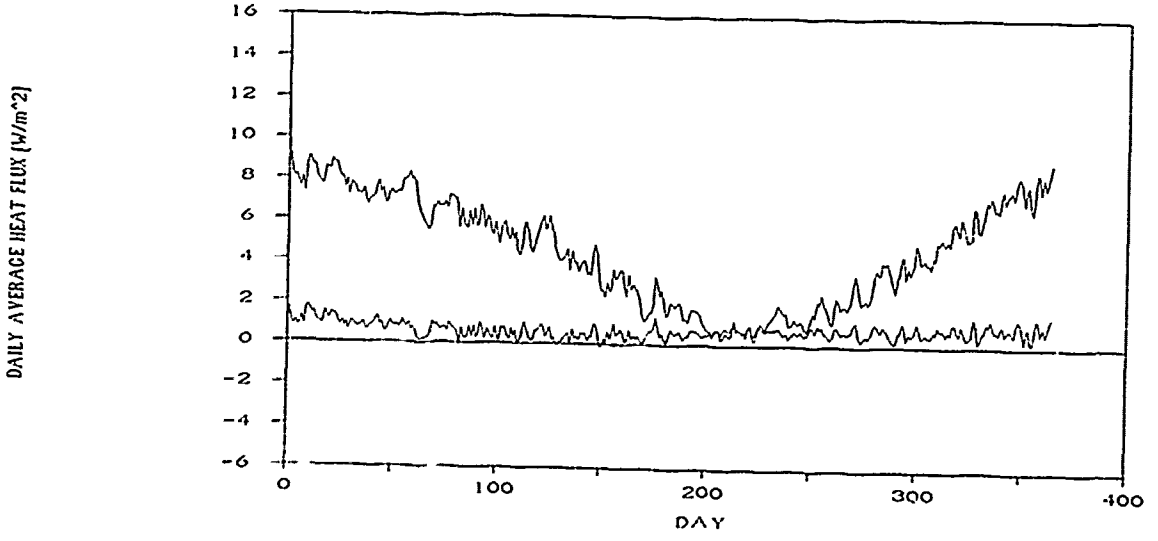

Figure 23. Heat flux--$T_f = T_{oa}$, Medford, OR.

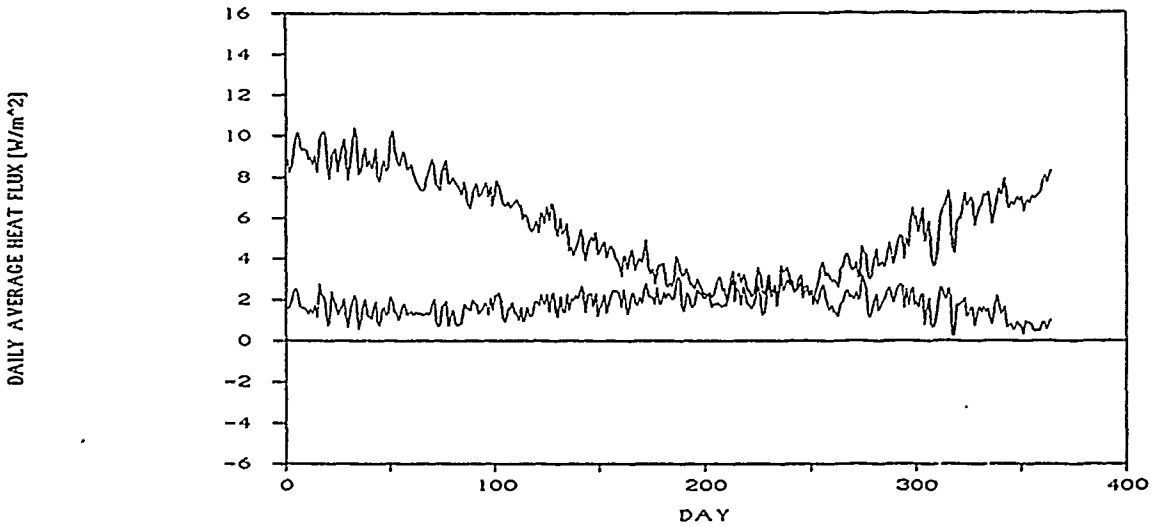

Figure 24. Heat flux--$T_f = T_{oa}$, Philadelphia, PA.

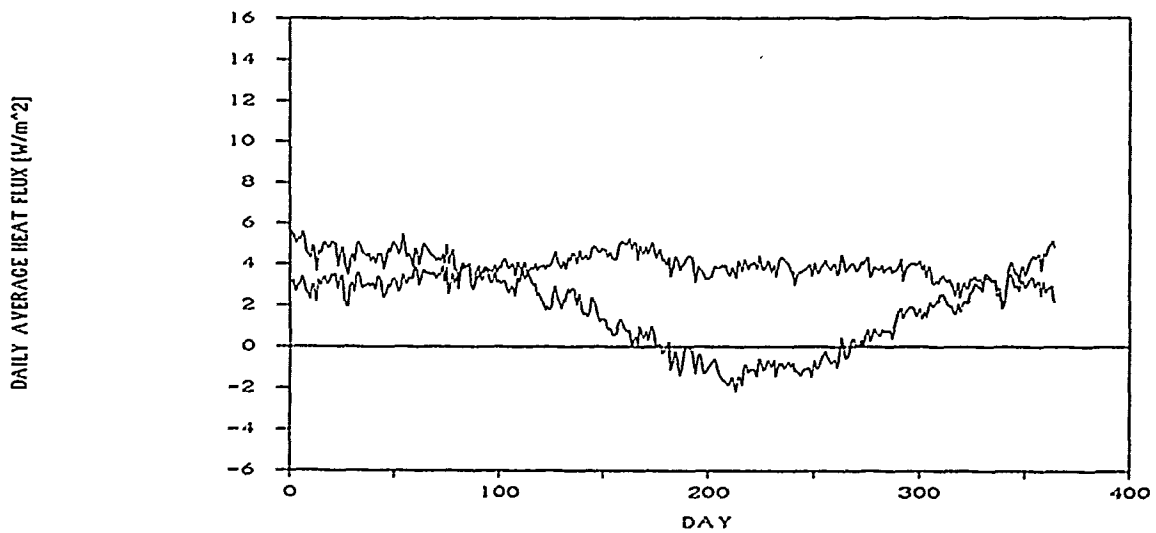

Figure 25. Heat flux--$T_f = T_{oa}$, Phoenix, AZ.

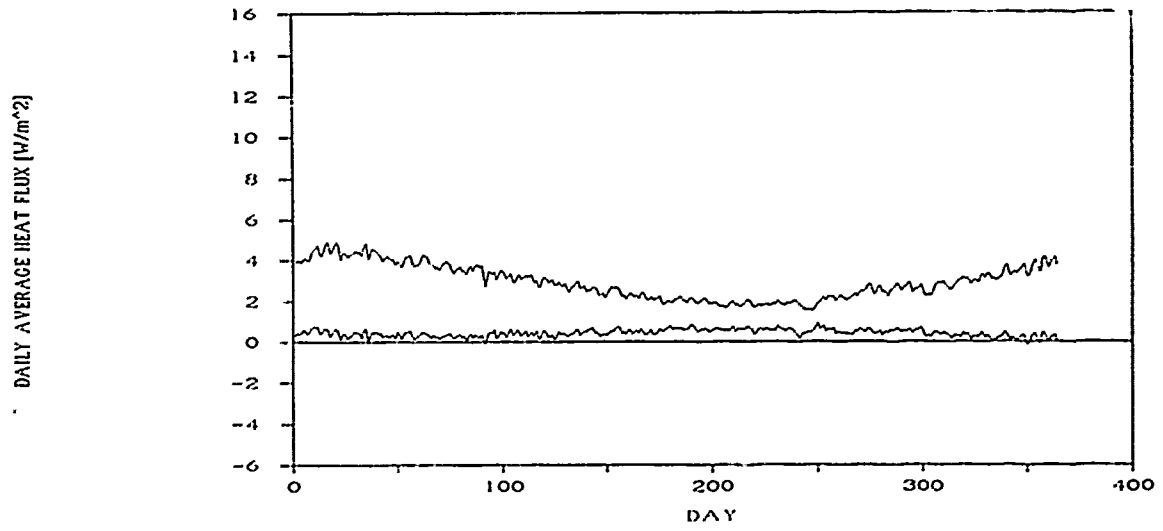

Figure 26. Heat flux--$T_f = T_{oa}$, 45 by 45, Minneapolis, MN.

Table 15

Results of Substituting Constant Indoor Air Temperature for Daily Average Slab Surface Temperature*

Model	City	Edge Size (m^2)	Mean Flux (W/M^2)	% of Data Within 15% of FDM (%)	Total Annual Energy Consumption (kWhr)	% Error in Total Energy Consumption (%)	Total Annual Difference in Energy Consumption (kWhr)
FDM	Minn	12	6.13	---	7716.9	---	---
GTF	Minn	12	6.74	68	8480.0	+9.0	+763.1
FDM	Med	12	3.87	---	4867.1	---	---
GTF	Med	12	4.27	66	5967.6	+10.3	+1100.5
FDM	Phil	12	3.89	---	4893.7	---	---
GTF	Phil	12	4.29	62	5398.7	+10.3	+505.0
FDM	Phoe	12	-1.66	---	-2082.9	---	---
GTF	Phoe	12	-1.38	66	-1736.8	-16.6	+346.1
FDM	Minn	45	2.50	---	44167.7	---	---
GTF	Minn	45	2.47	99	43725.3	-1.0	-442.4

*FDM = Finite Difference Model; GTF = Ground Transfer Function.

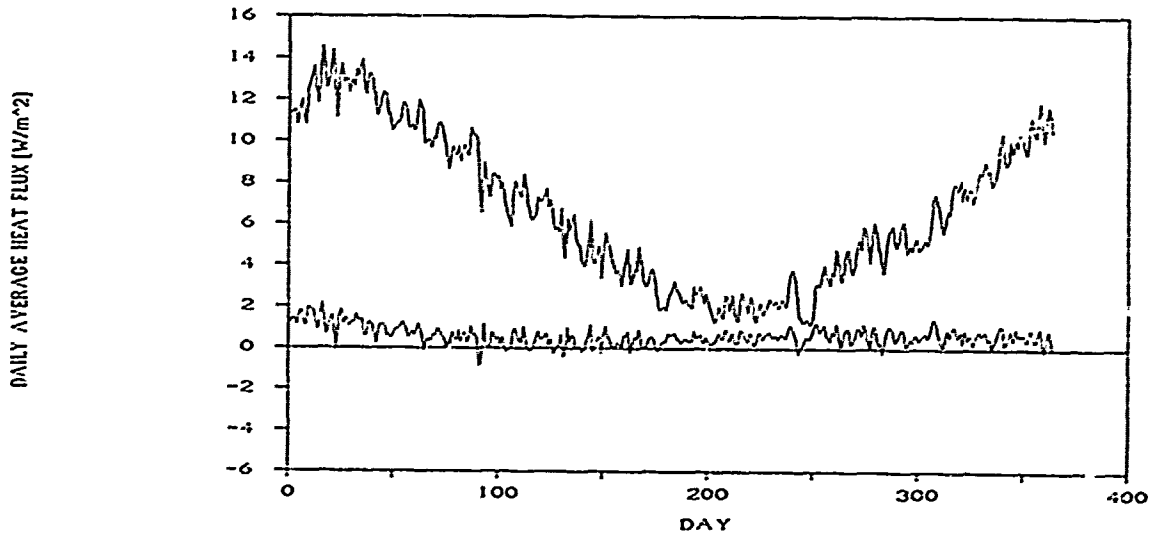

Figure 27. Heat flux--$T_b = T_{la}$, Minneapolis, MN.

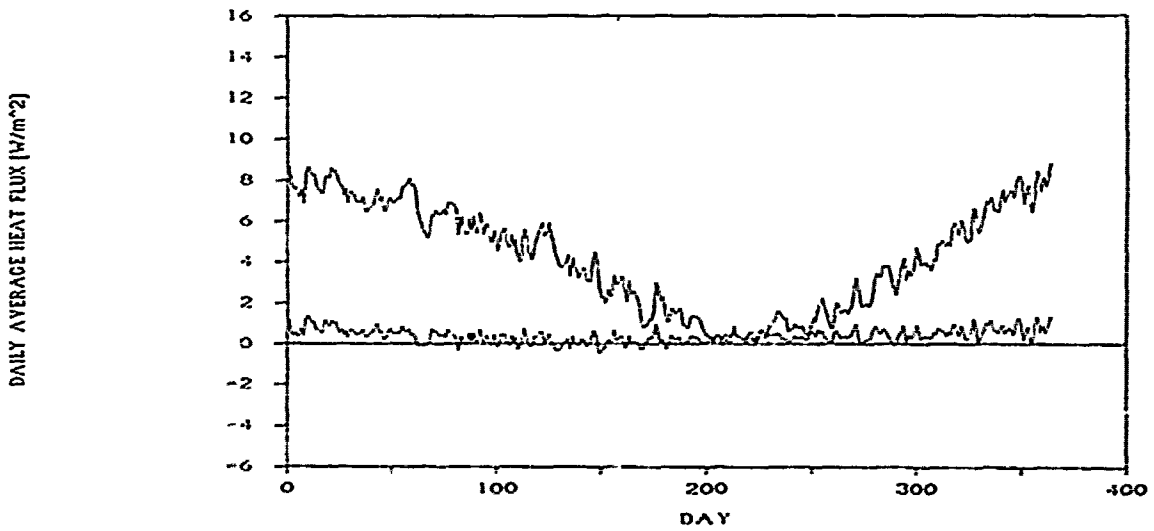

Figure 28. Heat flux, $T_b = T_{la}$, Medford, OR.

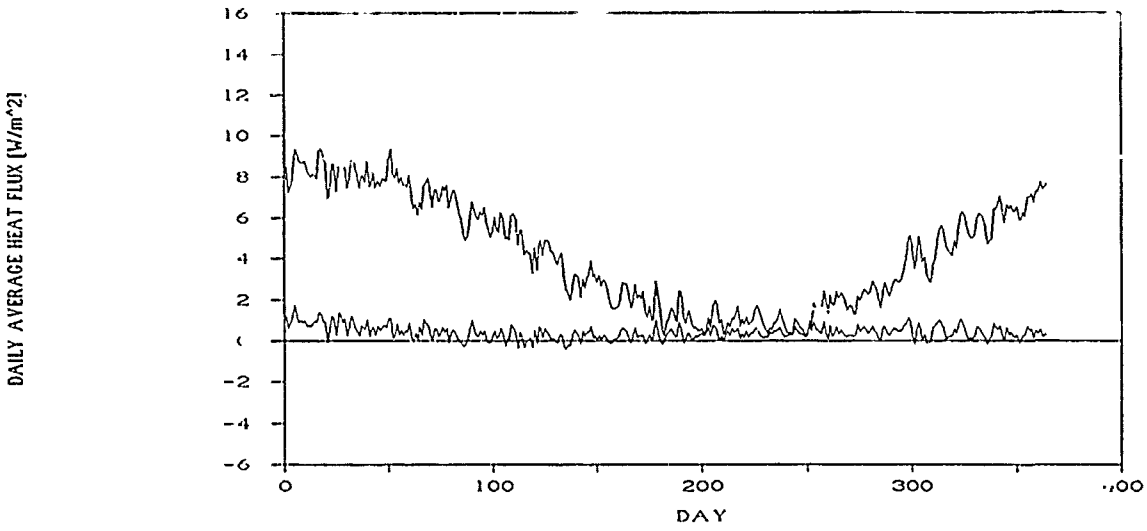

Figure 29. Heat flux--$T_b = T_{la}$, Philadelphia, PA.

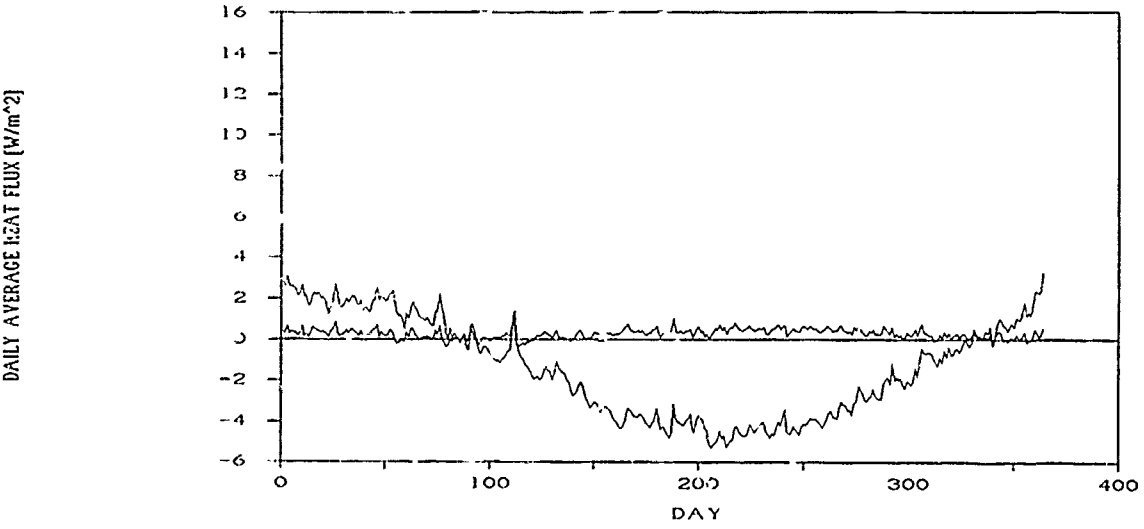

Figure 30. Heat flux--$T_b = T_{la}$, Phoenix, AZ.

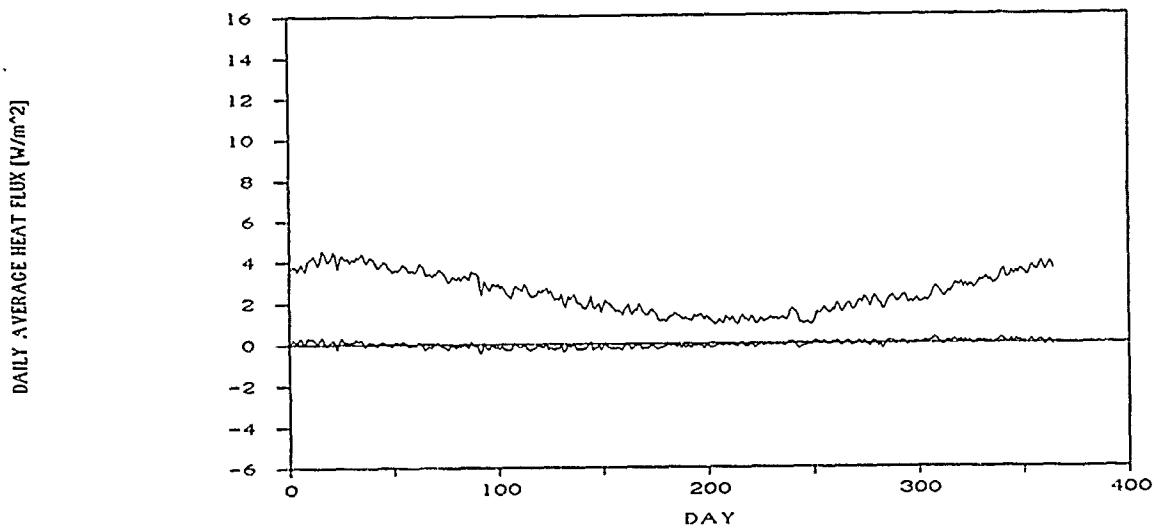

Figure 31. Heat flux--$T_b = T_{ia}$, 45 by 45, Minneapolis, MN.

Pairing the two square slabs and the two nonsquare slabs, a line was fit to each set and the coefficients of the resulting equations were compared.

It was clear that a single set of linear equations for the network parameters in terms of the slab area, perimeter, or characteristic length could be written and should give acceptable results for all four cases. A set of equations based on these data is suggested elsewhere.[57]

Using the original L matrix and the A and V matrices generated using the new set of linear equations, new GTFs and scalar constants were calculated and QCALC was used to calculate the daily average heat flux through the slab using the Minneapolis weather data. The results are shown in Figures 32 through 35. Table 16 gives numerical comparisons.

In all cases, more than 80 percent of the data are within 15 percent of the FDM data, and the error in total energy consumption is less than 10 percent. Clearly, it is possible to develop a set of equations for calculating network parameters as functions of slab area, perimeter, and characteristic length that give good results for a variety of rectangular geometries. The equations developed for this example cannot be considered universal; a more rigorous method of parameter estimation should be used to develop a truly generic parameter set. However, this example indicates that such a procedure should yield good results.

[57]J.A. Amber.

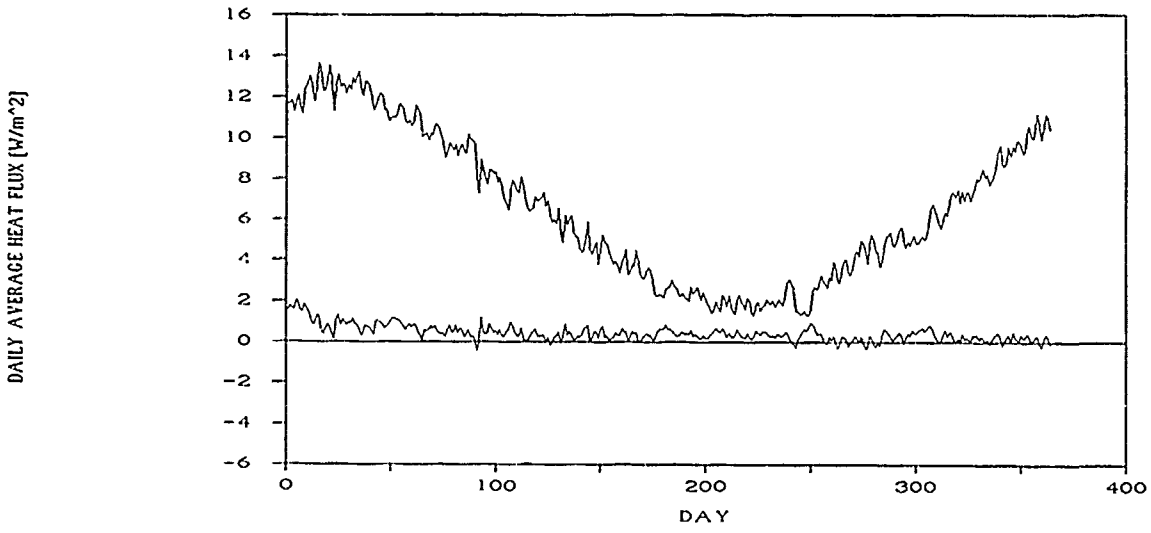

Figure 32. Heat flux--12 by 12.

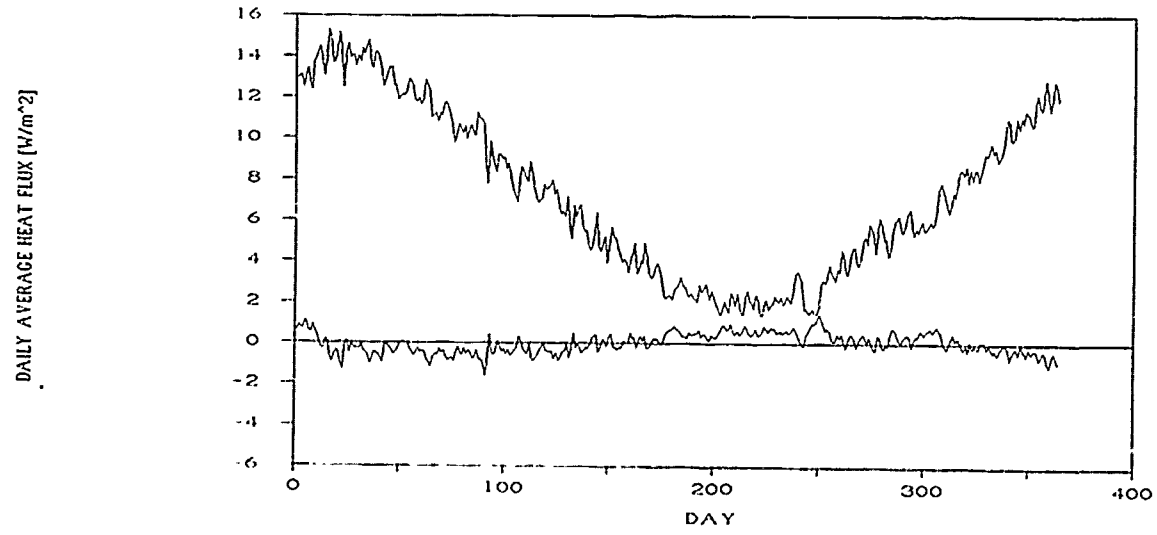

Figure 33. Heat flux--6 by 24.

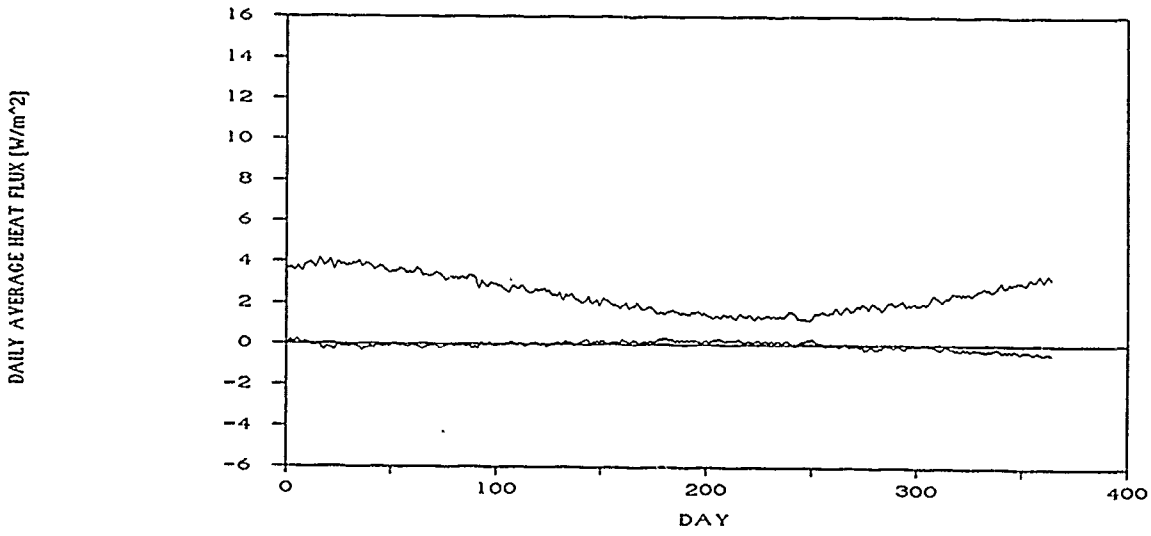

Figure 34. Heat flux--45 by 45.

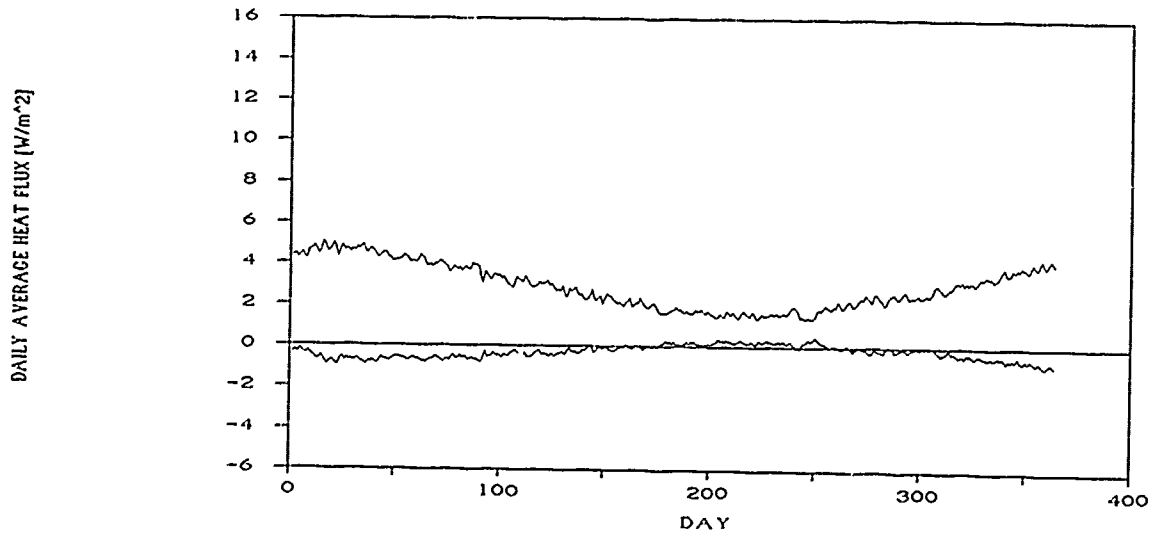

Figure 35. Heat flux--18 by 112.

Table 16

Results of GTF Model Using Parameter Sets Based on Empirical Equations*

Model	Slab Size (m^2)	Mean Flux (W/M^2)	% of Data Within 15% of FDM (%)	Total Annual Energy Consumption (kWhr)	% Error in Total Energy Consumption (%)	Total Annual Difference in Energy Consumption (kWhr)
FDM	12 x 12	6.10	---	7716.9	---	---
GTF	12 x 12	6.57	80	8263.1	+6.6	+546.2
FDM	6 x 24	7.30	---	9180.2	---	---
GTF	6 x 24	7.31	81	9190.5	+0.1	+10.3
FDM	45 x 45	2.50	---	44167.7	---	---
GTF	45 x 45	2.47	93	43763.6	-0.9	-404.1
FDM	18 x 112	3.19	---	56405.2	---	---
GTF	18 x 112	2.93	86	51765.1	-8.2	-4640.1

*FDM = Finite Difference Model; GTF = Ground Transfer Function.

5 CONCLUSIONS AND RECOMMENDATIONS

This report has described the development of two potentially useful methods for estimating heat transfer through slab-on-grade floors. one appropriate for manual calculations and the other suited for use in transfer function-based energy analysis programs. Data from an extensive program of three-dimensional numerical simulations provided fundamental information for the formulation and testing of these models. The conclusions and recommendations presented below rest on analysis of the numerical data base (above and in USACERL TM E-89/11) and on the performance of the proposed models.

Slab Heat Loss Characteristics

Temporal and Spatial Characteristics

This study generally supports previous qualitative findings concerning the soil temperature distribution near a slab-on-grade and the floor heat transfer regime:

- Temperature and heat flux distributions in the perimeter zone are essentially independent of floor size for a given foundation design.
- Core conditions depend on the size and shape of a building. Floor center heat flux may vary by a factor of two or three from a small building to a large one.
- Variations in floor total heat loss on a time scale shorter than 24 hr appear to be insignificant for general-purpose calculations. Hourly effects on perimeter zones, however, may be of consequence in passive design.
- Seasonal variations in the soil temperature regime cause heat loss to be more uniform over the surface of a floor in the summer than during the winter. This fact makes perimeter loss coefficient methods unacceptable for purposes other than heating load calculations. They are not suitable for annual energy consumption estimates.

Geometric Effects

The results of this study indicate that influences of shape and size on floor heat loss in three dimensions can be related to the effect of the characteristic length A/P on heat loss per unit area for rectangular and L-shaped floor plans. Given the nature of this relationship, there is every reason to expect that it extends to more arbitrarily defined shapes, as well.

Analysis using Eq 26 showed that floor area strongly influences the mean component of heat loss but has little impact on the periodic component. Consequently, heat loss from floors with large A/P may exceed F_2 method predictions based on small floor results by as much as a factor of two. On the basis of this work, the F_2 method is not trustworthy.

Since two-dimensional heat transfer from a slab corresponds to the three-dimensional, infinite aspect ratio case (for which A/P = L/2), there is an equivalent two-dimensional case for any three-dimensional floor. This mapping is potentially of great significance, since it permits the heat loss from any number of arbitrarily shaped floors to be obtained from the heat loss of a single two-dimensional case with the same A/P value.

Climate Effects

Differences in heat loss related directly to differences in the mean and amplitude of ground surface temperature. Air temperature is unreliable as a reference because of the wide variation in local soil temperature that may result from differences in surface conditions.

Ground Surface Boundary Condition Effects

Potential evapotranspiration caused mean ground temperature to fall several degrees below mean air temperature and also decreased the amplitude of the annual cycle. The effect was most pronounced during the summer when evapotranspiration potential is highest. Without a latent loss component at the ground surface, the mean and amplitude of surface temperature increased substantially and ground temperature exceeded air temperature through most of the year. The difference between air and surface temperatures in the "no evapotranspiration" case also was greatest during the summer because of the effect of greater solar gain.

Evapotranspiration increased maximum floor heat loss by 4 to 11 percent relative to the zero latent loss case for a representative group of runs from Philadelphia, Medford, and Minneapolis while the corresponding Phoenix simulation showed a change of nearly 50 percent. Mean values were affected to an even greater extent. For Philadelphia, Medford, and Minneapolis, mean heat loss decreased by 18 to 32 percent when evapotranspiration was suppressed. Phoenix mean heat loss changed by 170 percent--from a net loss to a net gain.

On the basis of this study, it must be concluded that the possible effects of latent heat loss on soil temperature are substantial. A boundary condition that includes radiation but neglects evaporation will predict ground surface temperatures that are generally elevated above air temperature during the day, sometimes by 10 °C or more. Conversely, a boundary condition that includes potential evapotranspiration will predict lower daytime ground temperatures and a lower mean. The use of ground surface conditions to modify loads on conventional buildings apparently has not been studied. Speltz and Meixel, however, have shown that earth-covered roofs can greatly reduce cooling loads.[58]

Soil Property Effects

Soil thermal conductivity has a profound effect on both the mean and transient components of heat loss. With the exception of foundation design, it is clearly the most crucial parameter affecting heat loss. Reliable estimates of slab-on-grade heat loss without consideration of soil conductivity are impossible. In this study, variation of soil conductivity produced greater change in heat loss than did variation in climate. Factor of two changes in conductivity, which may occur in the field, produced comparable changes in heat loss. Thermal diffusivity of the soil, however, did not exert much influence on floor heat loss over the range of values considered.

Insulation Effects

The area dependence of the heat loss from an insulated floor was greater than that of the same floor without insulation because insulation made floor temperature and heat loss more uniform. This finding casts suspicion on the validity of F_2 method heat loss predictions for highly insulated floors. A comparison of observed heat loss values with current U. S. Army design energy targets for residential and office space types[59] showed that the annual energy consumption of an uninsulated floor

---

[58]J. J. Speltz and G. D. Meixel.

[59]*Architectural and Engineering Instructions: Design Criteria* (Office of the Chief of Engineers, 13 March 1987).

could be as much as 30 to 50 percent of the energy budget for new construction. Perimeter insulation can reduce this contribution by as much as 50 percent, and perhaps more. The contribution of the floor load decreases with size because average flux falls as A/P increases.

Modeling Guidelines

The results of this study show that an accurate model of slab-on-grade heat loss will, as a minimum, account for the following:

- Soil thermal conductivity
- Surface boundary effects on soil temperature
- Foundation design and insulation treatment
- Area effects (A/P dependence of average heat flux).

Neglect or improper specification of any of these items could cause predictions to err by 50 percent or more. In addition, manual methods should use soil temperature as an environmental reference and distinguish between the mean and periodic components of heat loss.

Evaluation of Candidate Models

Characteristic Length Method

The method derived and discussed in Chapter 3 is well suited to use as a manual or simplified computer technique. It is compact, easy to apply, applicable year-round, and is more consistent with detailed numerical predictions than is the F_2 method. Because it incorporates the A/P scaling discovered through study of the numerical data base, this model can be used for floors of relatively arbitrary shape and size. Because it is valid all year, it can be used for simplified energy analyses as well as for load calculations. The model is limited to the extent that, in application, it requires multiple coefficient sets.

The primary task required to make the proposed model usable is the computation of enough sets of model coefficients (c_1, d_1, c_2, and d_2) to permit application across the anticipated range of soil properties and foundation types. The precise size of this task, which would be considerable, would be determined by considerations of acceptable accuracy as well as by the variety of foundation types judged significant. In support of the model, it would also be necessary to provide the user with either ground-surface temperature model coefficients corresponding to a range of surface boundary conditions or the software to compute them. Neither option would be time-consuming or difficult.

Transfer Function Model

A simple multiple-input transfer function model of the heat transfer in the ground under a square slab was presented. It was tested and modified to model both relatively small slabs where edge effects are strong and larger slabs where heat flux is more strongly affected by the flux through the core. Tested over a broad range of climatic conditions, the model calculated daily averaged slab heat flux within 1 W/m^2 at all times and for all locations. This result translates to an error of less than 1 percent (compared with the detailed finite difference model) for moderate and cold climates and 12 percent for Phoenix where the total flux is very low. The model's accuracy depends on the accuracy of the input data; however, some reasonable approximations to the necessary input data can give acceptable results. A preliminary study of the development of network parameters based on slab characteristic length indicated that the transfer function model has the potential to model more complex systems accurately.

Because of its conceptual similarity to existing energy analysis programs that use transfer function models of building components, the model presented in Chapter 4 may be particularly suitable for incorporation into such programs. This model also could serve as part of a stand-alone slab heat loss program in situations for which the daily average slab surface temperatures are known or can be reasonably approximated. In either stand-alone or integrated form, the model would require input from some source of soil temperature data.

Recommendations

As noted above, the commonly used design techniques for slab-on-grade heat loss, such as the F_2 method, are seriously limited in applicability and represent an obsolete view of earth-coupled heat loss. Because of the increased importance of building/ground thermal interactions in contemporary construction, it is imperative that the methods for earth-coupled heat transfer analysis be upgraded to reflect the current state of knowledge. This objective could be met both through the development of better manual methods and through computer-aided design tools.

The full capability of the transfer function model was not tested in this study. Further work is recommended to expand the use of the model to nonsquare and possibly even nonrectangular surfaces through a definition of the network parameters based on characteristic length. Testing and possibly modification of the parameter equations to support differential slab core and slab edge temperatures would allow the model to be used more effectively for insulation studies.

Both the manual A/P and transfer function approaches should be extended to include additional earth-coupled surfaces such as bermed walls, basements, and heated slabs. More research is needed into the effects of soil property variation and moisture movement.

REFERENCES

Andersland, O. B., and D. M. Anderson, *Geotechnical Engineering for Cold Regions* (McGraw-Hill, 1978).

Architectural and Engineering Instructions: Design Criteria (Office of the Chief of Engineers, 13 March 1987).

Amber, J. A., *Multiple-Input Transfer Function Model of Heat Transfer From Square Slab Floors*, M. S. Thesis (University of Illinois, May 1989; also published as USACERL Technical Manuscript E-90/01/ADA219193 (November 1989).

Bahnfleth, W. P., *Three-Dimensional Modeling of Heat Transfer From Slab Floors*, Ph.D. Thesis (University of Illinois at Urbana-Champaign, May 1989); also published as USACERL Technical Manuscript E-89/11/ADA210826 (July 1989).

Bahnfleth, W. P., P. H. Shipp, T. Kasuda, and J. W. Bean, "Simplified Methods for Determining Seasonal Heat Loss From Uninsulated Slab-on-Grade Floors,"*ASHRAE Transactions*, Vol 90 (1984).

Bareither, H. D., A. N. Fleming, and B. E. Alberty, *Temperature and Heat Loss Characteristics of Concrete Floors Laid on the Ground*, Technical Report PB 93920 (University of Illinois Small Homes Council, 1948).

Ceylan, H. T., and G. E. Myers, "Long-Time Solutions to Heat-Conduction Transients With Time-Dependent Inputs," *ASME Journal of Heat Transfer*, Vol 102 (February 1980).

Dill, R. S., W. C. Robinson, and H. D. Robinson, *Measurements of Heat Losses From Slab Floors*, Building Materials and Structures Report BMS103 (National Bureau of Standards, 1943).

Eckert, E. R. G. and E. Pfender, "Heat and Mass Transfer in Porous Media With Phase Change," *Proceedings, 6th International Heat Transfer Conference* (1978).

Geiger, R., *The Climate Near the Ground* (Harvard University Press, 1961).

Gilpin, R. R. and B. K. Wong, "Heat-Valve'" Effects in the Ground Thermal Regime," *ASME Journal of Heat Transfer*, Vol 98 (1976).

Gold, L. W., "Influence of Surface Conditions on Ground Temperature," *Canadian Journal of Earth Sciences*, Vol 4 (1967).

Hittle, D. C., *Calculating Building Heating and Cooling Loads Using the Frequency Response of Multilayered Slabs*, Technical Manuscript E-169/ADA097597 (USACERL, February 1981).

Jensen, M. E. (Ed.), *Consumptive Use of Water and Irrigation Water Requirements* (American Society of Civil Engineers, 1973).

Kersten, M. S., *Thermal Properties of Soils*, Bulletin No. 28, Vol LII, No. 21 (University of Minnesota Institute of Technology Engineering Experiment Station, June 1, 1949).

Kreith, F., and W. D. Sellers, "General Principles of Natural Evaporation," *Heat and Mass Transfer in the Biosphere, Part I: Transfer Processes in the Plant Environment*, D. A. de Vries and N. H. Afgan (Eds.) (Wiley, 1975).

Kung, E. C., R. A. Bryson, and D. H. Lenschow, "A Study of Continental Surface Albedo on the Basis of Flight Measurements and Structure of the Earth's Surface Cover Over North America," *Monthly Weather Review*, Vol 92, No. 12 (1964).

Kusuda, T., "The Effect of Ground Cover on Earth Temperature," *Alternatives in Energy Conservation. The Use of Earth Covered Buildings*, NSF-RA-760006, (National Science Foundation, 1975).

Kusuda, T., and J. W. Bean, "Simplified Methods for Determining Seasonal Heat Loss From Uninsulated Slab-on-Grade Floors," *ASHRAE Transactions*, Vol 90 (1984), part 1b.

Kusuda, T., and P. R. Achenbach, "Earth Temperature and Thermal Diffusivity at Selected Stations in the United States," *ASHRAE Transactions*, Vol 71 (1965), part 1.

Labs, K., "Regional Analysis of Ground and Above-Ground Climate," *Underground Space*, Vol 6, No. 6, and Vol 7, No. 1 (1982).

Labs, K., J. Carmody, R. Sterling, L. Shen, Y. J. Huang, and D. Parker, *Building Foundation Design Handbook*, DE88-013350 (DOE, May 1988).

MacDonald, G. R., D. E. Claridge, and P. A. Oatman, "A Comparison of Seven Basement Heat Loss Calculation Methods Suitable for Variable-Base Degree-Day Calculations," *ASHRAE Transactions*, Vol 91 (1985), part 1b.

Moreland, F., F. Higgs, and J. Shih (Eds.), *Earth Covered Buildings: Technical Notes*, US-DOE CONF-7806138-P1 (DOE, 1979).

1989 ASHRAE Fundamentals-SI Version (American Society of Heating, Refrigerating, and Air-Conditioning Engineers [ASHRAE], 1989).

Patankar, S. V., *Numerical Heat Transfer and Fluid Flow* (Hemisphere, 1980).

Sellers, W. D., *Physical Climatology* (University of Chicago Press, 1965).

Sellers, W. D., and P. S. Dryden, *An Investigation of Heat Transfer From Bare Soil*, Final Report, Grant No. DA-AMC-28-043-66-G27 (University of Arizona, April 1967).

Seem, J. E., *Modeling of Heat Transfer in Buildings*, Ph.D. Thesis (University of Wisconsin, 1987).

Shen, L. S , J. Poliakova, and Y. J. Huang, "Calculation of Building Foundation Heat Loss Using Superposition and Numerical Scaling," *ASHRAE Transactions* Vol 94 (1988), part 2.

Shipp, P. H , *The Thermal Characteristics of Large Earth-Sheltered Structures*, Ph.D. Thesis (University of Minnesota, 1979).

Speltz, J. J., *A Numerical Simulation of Transient Heat Flow in Earth Sheltered Buildings for Seven Selected U.S. Cities*, M.S. Thesis (Trinity University, 1980).

Speltz, J. J., and G. D. Meixel,"A Computer Simulation of the Thermal Performance of Earth Covered Roofs," *Proceedings, Underground Space Conference and Exposition*, Kansas City, MO (June 1981).

APPENDIX:

DATA SET USED TO EVALUATE PROPOSED MODELS

Series G

Rectangular and L-shaped plans. Evapotranspiration on, shadowing off. Medford, OR weather. Base case properties (k = 1W/m-K, density = 1200 Kg/m^3, specific heat = 1200 J/m^3-K). Variable aspect ratio for areas of 144 m^2, 900 m^2, 2025 m^2, and 3600 m^2. All floors are 0.1 m thick. Soil temperature is 11.7 °C at a depth (z_{max}) of 10 m or 15 m, as indicated. Side boundaries are approximately 12 m beyond the edge of the slab. The purpose of this series is to demonstrate geometric influences on heat loss.

ID	Plan Shape	Dimensions(m)	Area (m^2)	Comments
GR01	rectangle	12 x 12	144	z_{max}=10 m
GR1A	rectangle	12 x 12	144	z_{max}=15 m
GR02	rectangle	8.5 x 17	144.5	z_{max}=10 m
GR03	rectangle	7 x 20.5	143.5	z_{max}=10 m
GR04	rectangle	6 x 24	144	z_{max}=10 m
GR05	rectangle	45 x 4	2025	z_{max}=10 m
GR5A	rectangle	45 x 45	2025	XMAX&YMAX>GR05
GR5B	rectangle	45 x 45	2025	z_{max}=15 m
GR06	rectangle	32 x 63	2016	z_{max}=10 m
GR6A	rectangle	32 x 63	2016	z_{max}=15 m
GR07	rectangle	23 x 88	2024	z_{max}=10 m
GR7A	rectangle	23 x 88	2024	z_{max}=15 m
GR08	rectangle	18 x 112	2016	z_{max}=10 m
GR8A	rectangle	18 x 112	2016	z_{max}=15 m
GR09	rectangle	30 x 30	900	z_{max}=10 m
GR9A	rectangle	30 x 30	900	z_{max}=15 m
GR10	rectangle	20 x 45	900	z_{max}=10 m
GR10A	rectangle	20 x 45	900	z_{max}=15 m
GR11	rectangle	17 x 53	901	z_{max}=10 m
GR11A	rectangle	17 x 53	901	z_{max}=15 m
GR12	rectangle	15 x 60	900	z_{max}=10 m
GR12A	rectangle	15 x 60	900	z_{max}=15 m
GR13	rectangle	60 x 60	3600	z_{max}=10 m
GR13A	rectangle	60 x 60	3600	z_{max}=15 m
GR14	rectangle	30 x 120	3600	z_{max}=10 m
GR14A	rectangle	30 x 120	3600	z_{max}=15 m
GR15	rectangle	20 x 180	3600	z_{max}=10 m
GR15A	rectangle	20 x 180	3600	z_{max}=15 m
GR16	rectangle	20 x 20	400	z_{max}=10 m
GR16A	rectangle	20 x 20	400	z_{max}=15
GR17	rectangle	10 x 40	400	z_{max}=10 m
GR17A	rectangle	10 x 40	400	z_{max}=10 m
GL01	L-shaped	******	144.9	z_{max}=15 m

GL02	L-shaped	******	2028	z_{max}=10 m
GL2A	L-shaped	******	2028	z_{max}=15 m
GL03	L-shaped	******	897.9	z_{max}=10 m
GL3A	L-shaped	******	897.9	z_{max}=15 m

Series W

Rectangular plans. The basic decks are taken from the previous series. The only factor varied was the weather file. TMY files from Minneapolis, MN, Phoenix, AZ, and Philadelphia, PA were used.

ID	Plan Shape	Dimensions (m)	Area(m^2)	Location
WMN1	rectangle	12 x 12	144	Minneapolis
WMN2	rectangle	45 x 45	2025	Minneapolis
WMN3	rectangle	6 x 24	144	Minneapolis
WMN4	rectangle	18 x 112	2016	Minneapolis
WPX1	rectangle	12 x 12	144	Phoenix
WPX2	rectangle	45 x 45	2025	Phoenix
WPX3	rectangle	6 x 24	144	Phoenix
WPX4	rectangle	18 x 112	2016	Phoenix
WPH1	rectangle	12 x 12	144	Philadelphia
WPH2	rectangle	45 x 45	2025	Philadelphia
WPH3	rectangle	6 x 24	144	Philadelphia
WPH4	rectangle	18 x 112	2016	Philadelphia

Series S

These runs show the effect of shade cast on the ground by a building. Sites are Medford and Phoenix. 15-m deep domain. Evapotranspiration is included except as noted.

ID	Plan Shape	Dimensions (m)	Area (m^2)	Location
SMD1	rectangle	12 x 12	144	Medford
SMD2	rectangle	6 x 24	144	Medford, Long E/W
SMD3	rectangle	6 x 24	144	Medford, Long N/S
SMD4	rectangle	12 x 12	144	Medford, No evap.
SPX1	rectangle	12 x 12	144	Phoenix

Series K

These runs show the effect of thermal conductivity and thermal diffusivity. They are identical to the "W" runs for Philadelphia except that the soil properties have been changed.

A. k = 2 W/m-K, density = 1700 kg/m^3, and specific heat = 1700 J/m^3-K.

ID	Plan Shape	Dimensions (m)	Area (m^2)	Location
KPH1	rectangle	12 x 12	144	Philadelphia
KPH2	rectangle	45 x 45	2025	Philadelphia
KPH3	rectangle	6 x 24	144	Philadelphia
KPH4	rectangle	18 x 112	2016	Philadelphia

B. k = 1 W/m-K, density = 1700 kg/m^3, and specific heat = 1700 J/m^3-K.

ID	Plan Shape	Dimensions (m)	Area (m^2)	Location
KPH5	rectangle	12 x 12	144	Philadelphia
KPH6	rectangle	45 x 45	2025	Philadelphia
KPH7	rectangle	6 x 24	144	Philadelphia
KPH8	rectangle	18 x 112	2016	Philadelphia

C. k = 0.5 W/m-K, density = 1200 kg/m^3, and specific heat = 1200 J/m^3-K.

ID	Plan Shape	Dimensions (m)	Area (m^2)	Location
KPH9	rectangle	12 x 12	144	Philadelphia
KPH10	rectangle	45 x 45	2025	Philadelphia
KPH11	rectangle	6 x 24	144	Philadelphia
KPH12	rectangle	18 x 112	2016	Philadelphia

D. k = 2 W/m-K, density = 1500 kg/m^3, and specific heat = 1500 J/m^3-K.

ID	Plan Shape	Dimensions (m)	Area (m^2)	Location
KPH13	rectangle	12 x 12	144	Philadelphia
KPH14	rectangle	45 x 45	2025	Philadelphia
KPH15	rectangle	6 x 24	144	Philadelphia
KPH16	rectangle	18 x 112	2016	Philadelphia

Series E

These runs show the effect of turning off evaporation in the surface boundary condition. Otherwise, they are the same as the corresponding series G and W runs.

ID	Plan Shape	Dimensions (m)	Area (m^2)	Location
EMN1	rectangle	12 x 12	144	Minneapolis
EMN2	rectangle	6 x 24	144	Minneapolis
EMN3	rectangle	45 x 45	2025	Minneapolis
EMN4	rectangle	18 x 112	2016	Minneapolis
EMD1	rectangle	12 x 12	144	Medford
EPH1	rectangle	12 x 12	144	Philadelphia
EPX1	rectangle	12 x 12	144	Phoenix

Series I

These runs indicate the effect of under-slab insulation. The insulating material is 2 in. extruded polystyrene board, k = 0.029 W/m-K. The resistance of 1- and 2-in. layers is 0.8759 and 1.75 K/(W/m^2), respectively. Two treatments are considered: edge + 1 m under slab, and edge + full under slab. Since insulation is applied primarily to mitigate heating load, Minneapolis weather is used in these runs.

ID	Plan Shape	Dimensions (m)	Area(m^2)	Location
IMN1	rectangle	12 x 12	144	2", 1 m strip
IMN2	rectangle	12 x 12	144	2", full
IMN3	rectangle	45 x 45	2025	2", 1 m strip
IMN4	rectangle	45 x 45	2025	2", full
IMN5	rectangle	6 x 24	144	2", 1 m strip
IMN6	rectangle	18 x 112	2016	2", 1 m strip
IMN7	rectangle	12 x 12	144	1", 1 m strip
IMN8	rectangle	12 x 12	144	1", full
IMN9	rectangle	45 x 45	2025	1", 1 m strip
IM10	rectangle	45 x 45	2025	1", full
IM11	rectangle	6 x 24	144	1", 1 m strip
IM12	rectangle	18 x 112	2016	1", full

Series Z

Rectangular plans. The basic decks are the same as WMN1-4. The only factor varied is the deep ground boundary condition. The ground temperature file has a zero-flux condition at a depth of 15m. Evapotranspiration is on.

ID	Plan Shape	Dimensions(m)	Area(m^2)	Location
ZMN1	rectangle	12 x 12	144	Minneapolis
ZMN2	rectangle	45 x 45	2025	Minneapolis
ZMN3	rectangle	6 x 24	144	Minneapolis
ZMN4	rectangle	18 x 112	2016	Minneapolis